Supplementary Information

Copolyesters with Branched Structures for Simultaneous Fluorescence and Resilience

Caohong Chen, Fei Liu*, Lili Zheng, Xiangting Zhao, Siqi Yu, Kangpeng Liu, Xiaoqin Jiang, Jinggang Wang*, Jin Zhu

Key Laboratory of Bio-based Polymeric Materials of Zhejiang Province, Ningbo Institute of Materials Technology and Engineering, Chinese Academy of Sciences, Ningbo, 315201, China.

** Corresponding Authors:*

Dr. Fei Liu, liufei@nimte.ac.cn;

Dr. Jinggang Wang, wangjg@nimte.ac.cn

Tel: +86-574-86685120, Fax: +86-574-86685186

Materials and Methods

Materials

1,4-Butanediol (BDO, 99.0%), Dimethyl terephthalate (DMT, 99.0%),1,3-Butanediol (1,3-BDO, 99%), Succinic anhydride (SAA, 99.0%), 1,3-Butanediol (1,3-BDO, 99.0%), Titanium (IV) butoxide (TBT，≥99.0%), and HPLC grade chloroform and $CDCl_3$ were bought from Sinopharm Chemical Reagent Co. Ltd (Shanghai, China). *Candida antarctica* lipase B (CALB) was offered by Novozymes Investment Co. Ltd. (Beijing, China).

Preparation of SBS Monomers

Scheme S1. Synthesis of SBS Monomers.

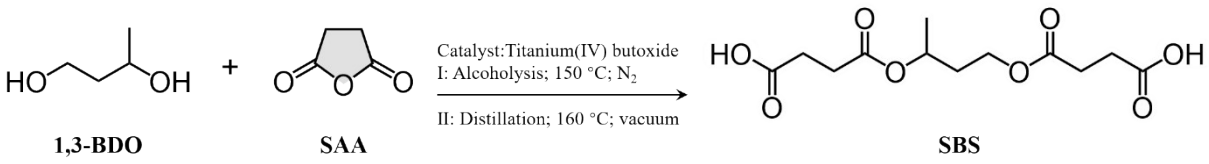

As illustrated in **Scheme S1**, the monomer was synthesized via a two-step method, which involves an alcoholysis ring-opening reaction and a vacuum distillation reaction. The experiment was conducted in a 3.0 L round-bottom flask equipped with an overhead mechanical stirrer. A typical experimental procedure is as follows: 205.1 g (2.05 mol) of succinic anhydride (SAA), 90.1 g (1.0 mol) of 1,3-butanediol (1,3-BDO), and 510.5 mg (0.15 mol% relative to 1,3-BDO) of tetrabutyl titanate (TBT) were charged into the flask. The flask was then evacuated to a vacuum of approximately 10 Pascals (Pa), sealed, and purged with dry, high-purity nitrogen to remove air and moisture. This purging process was repeated three times. The alcoholysis ring-opening reaction was carried out at 150 °C for 4.0 hours under a nitrogen atmosphere. After the reaction was completed, the vacuum distillation reaction was performed under a vacuum of less than 15 Pascals (Pa). After 2 hours of reaction, a yellow liquid with a purity of 99% was obtained.

$$\text{SBS mol\%} = \frac{2I_g}{2I_g + I_{SAA}} \times 100\% \qquad \textbf{Equation S1}$$

Preparation of PBST copolyesters

As illustrated in **Scheme S2**, the copolyesters were synthesized via a two-stage melt polymerization method, which involves esterification and polycondensation reactions. The experiment was conducted in a 3.0-liter (L) round-bottom flask equipped with an overhead mechanical stirrer (**Scheme S2**). A typical experimental procedure is as follows: 50.5 grams (g, 0.56 moles/mol) of 1,4-butanediol (BDO), 42.6 grams (g, 0.24 moles/mol) of dimethyl terephthalate (DMT), 46.4 grams (g, 0.16 moles/mol) of SBS, and 204.2 milligrams (mg, 0.15 mol% relative to SA) of tetrabutyl titanate (TBT) were charged into the flask. The flask was then evacuated to a vacuum of approximately 10 Pascals (Pa), sealed, and purged with dry, high-purity nitrogen to remove air and moisture. This purging process was repeated three times. The esterification reaction was carried out at 180-200 degrees Celsius (℃) for 5.0 hours under a nitrogen atmosphere. Once the reaction reached the maximum theoretical yield, the temperature of the system was gradually increased to 240-260 degrees Celsius (℃) over a period of 1.5 to 2.0 hours, and maintained under a vacuum of less than 15 Pascals (Pa) for an additional 3.0 hours. Throughout the entire process, the stirring rate was consistently kept at 30-180 revolutions per minute (rpm).

A similar procedure was used to synthesize other PBST copolyesters with different number-average molecular weights (M_n) and molar ratios of BS segments. These synthesized compounds were designated as PBSTX, where "X" represents the content of BS segments, ranging from 0 to 50 mole percent (mol%).

Characterization

Molecular structure characterization

The chemical structure, composition, and BS segment content of the PBST copolyesters were characterized by proton (^{1}H) and carbon-13 (^{13}C) nuclear magnetic resonance (NMR) spectroscopy in trifluoroacetic acid (TFA) solvent. NMR measurements were performed at room temperature using a Bruker ADVANCE NEO 600 spectrometer operating at a resonance frequency of 600 MHz. Intrinsic viscosities ([η]) of the PBST copolyesters were determined at 30 °C using an Ubbelohde capillary viscometer (Type Ic, viscometer constant K = 0.03294). All viscosity measurements were conducted in a mixed solvent system consisting of phenol and

tetrachloroethane (50:50, w/w; Aladdin, analytical reagent grade) with a copolymer concentration of 5 mg/mL. Fourier transform infrared (FT-IR) spectroscopic analysis was carried out at room temperature using an Agilent Cary 660 + 620 FT-IR microspectrometer. Number-average molecular weights (M_n) and molecular weight distributions (Đ) of the PBST copolyesters were measured by gel permeation chromatography (GPC) using a PL-GPC 220 instrument. Chloroform ($CDCl_3$) was used as the eluent at a flow rate of 1.0 mL/min, and all GPC measurements were performed at 40 °C.

Differential scanning calorimetry (DSC): Differential scanning calorimetry (DSC) measurements were performed using a Mettler-Toledo DSC I instrument under a nitrogen atmosphere, following a standard temperature protocol consisting of a heating-cooling-reheating cycle. Both the heating and cooling rates were set to 10 °C min^{-1}, with a 5-min isothermal hold to erase the thermal history of the samples. For each measurement, approximately 5-8 mg of sample was loaded into an aluminum crucible. All heating and cooling curves were recorded and retained for subsequent analysis.

Thermo-gravimetric analys is (TGA): Thermal stability was evaluated using thermogravimetric analysis (TGA) on a Mettler-Toledo TGA/DSC simultaneous thermal analyzer. Samples with a mass of 5-6 mg were analyzed under both nitrogen and air atmospheres, with a gas flow rate of 40 mL min^{-1} maintained for each atmosphere. The samples were heated from 50 °C to 800 °C at a heating rate of 20 °C min^{-1}, and the TGA curves were recorded continuously throughout the heating process.

Dynamic Mechanical Analyzer (DMA): The dynamic mechanical properties of annealed PBST copolyesters were characterized using a dynamic mechanical analyzer (DMA Q800, TA Instruments). The measurements were performed in multi-frequency strain mode at a fixed frequency of 1 Hz, with the temperature ranging from −120 °C to just below the melting temperature (T_m) and a heating rate of 3 °C min^{-1}.

Mechanical Tests: Tensile strength, tensile modulus, and elongation at break were measured at room temperature using a Zwick/Roell Z1.0 universal testing machine equipped with a 1 kN load cell, at a crosshead speed of 100 mm min^{-1}. Dumbbell-shaped specimens with dimensions of 20.0 mm (length) × 2.0 mm (neck width) × 1.0 mm (thickness) were fabricated via hot press molding.

Cyclic tensile tests were performed to evaluate the elastic recovery capability of the PBST copolyesters through repeated loading-unloading cycles. All tests were conducted at 25 °C using a full-cycle protocol: specimens were stretched to a maximum strain (ε_m) of 200% and

100% at a rate of 100 mm min^{-1}, followed by retraction of the crosshead at a recovery rate of 50 mm min^{-1} until the applied load returned to 0 N. This loading-unloading cycle was repeated five times. The elastic recovery ratio (R_r) of the PBST copolyesters was calculated using **Equation S2.**

$$R_r(N) = \frac{\varepsilon_m - \varepsilon_p(N)}{\varepsilon_m - \varepsilon_p(N-1)} \qquad \textbf{(Equation S2)}$$

where N represents the number of cycles, ε_m denotes the maximum strain of samples, $\varepsilon_p(N)$ and $\varepsilon_p(N\text{-}1)$ are the strains of PECS copolyesters during two consecutive cycles when the standard load is 0 N, and the term $R_r(N)$ indicates the elastic recovery ratio of the Nth cycle.

Each sample was tested in parallel five times to ensure the reliability and accuracy of the experimental data.

Fatigue testing: Cyclic stretching curves at 200% strain were recorded over 1,000 repetitions using a Cellscale instrument. The initial length, neck width, and thickness of the film were set to 50, 10, and 0.3 mm, respectively.

Small Angle X-ray Scattering (SAXS): Small-angle X-ray scattering (SAXS) measurements were performed using a Xeuss 3.0 SAXS instrument (Xenocs, France) with monochromatic X-rays of wavelength 0.15 nm. The distance between the sample and detector was set to 1000 mm. According to Bragg's law, the position of the maximum scattering vector (q_{max}) corresponding to the characteristic peak correlates with the long period (L), as described by the equation: $L = 2\pi/q_{max}$. Herein, q is the scattering vector, defined by the standard equation $q = 4\pi(\sin\theta)/\lambda$ (a correction from the original erroneous expression); in this equation, λ is the X-ray wavelength, and θ is half of the scattering angle (2θ).

Fluorescence Measurements: Fluorescence emission wavelengths were measured in the range of 380-700 nm using a 150 W xenon (Xe) lamp fluorescence spectrometer (Model: FL3-111). The fluorescence excitation slit width was set to 4/3 nm, and the excitation wavelength was fixed at 360 nm. Quantum efficiency measurements were performed using a QE-2100 quantum efficiency tester (Otsuka, Japan). X-ray photoelectron spectroscopy (XPS) measurements were conducted with an AXIS SUPRA spectrometer to determine the binding energies of the fluorescent materials.

Cytotoxicity Assay: The cytotoxicity of PBST films was evaluated by assessing cell viability. Two PBST film samples (PBST30 and PBST40) were selected for the characterization. Circular specimens with a uniform diameter of 14 mm were cut from the films and sterilized. These sterilized specimens were then placed in sterile 24-well culture plates containing DMEM medium and pre-incubated overnight in a cell culture incubator. On the following day, fibroblasts (ZQ 0450, Zhongqiao Xinzhou Biotechnology, Shanghai, China) in the logarithmic growth phase (optimal growth state) were seeded onto the films. After the cells adhered to the film surfaces and initiated proliferation, cell viability was measured every 24 hours over a three-day period using the Cell Counting Kit-8 (CCK-8) assay. For each measurement, 10 μL of CCK-8 solution was added to each well, followed by incubation at 37 °C for 2 hours (n = 3). A control group, in which cells were cultured without PBST films, was also included in the experiment. After incubation, an appropriate volume of supernatant was transferred to a 96-well plate, and the optical density (OD) value was measured at a wavelength of 450 nm using a multi-functional microplate reader.

Hemolysis assays: In vitro hemocompatibility of PBST films was evaluated via hemolysis assays. A 4% suspension of rat red blood cells (RBCs) was prepared and aliquoted into 1.5 mL centrifuge tubes, each containing a circular PBST film specimen with a diameter of 6 mm. The samples were incubated at 37 °C for 2 h, followed by centrifugation at 5000 rpm for 10 min. The color and clarity of the supernatant were visually inspected, and aliquots of the supernatant were transferred to a 96-well plate for optical density (OD) measurement at 545 nm using a multi-functional microplate reader (Thermo Fisher Scientific, USA). Hemolysis rates were calculated from the obtained OD values to assess the hemocompatibility of the PBST films. Four experimental groups were set up: (1) positive control group with 1% Triton X-100; (2) blank control group with normal saline only; (3) PBST30 film group; and (4) PBST40 film group.

Degradation experiments: Enzymatic degradation experiments were performed in phosphate buffer solution (PBS) containing 0.1 mg mL^{-1} Candida Antarctica Lipase B (CALB). PBST film samples with dimensions of 10.0 mm (length) × 20.0 mm (width) × 0.35 mm (thickness) were used for the experiments. Additionally, the samples were washed with deionized water and subsequently dried under vacuum at 40 °C until a constant weight was achieved. The degradation degree was evaluated by the weight loss percentage, which was calculated using **Equation S3.**

$$\text{Weight loss (\%)} = \frac{w_0 - w_t}{w_0} \times 100\% \qquad \textbf{(Equation S3)}$$

where w_0 and w_t represent the weight of the samples before and after degradation, respectively.

The surface morphology of the degraded film samples was characterized using a high-resolution field-emission scanning electron microscope (SEM, Verios G4 UC). Prior to characterization, all samples were subjected to a 10 nm platinum sputtering treatment for approximately 120 s using an anion sputter coater (E-1045, Hitachi) to enhance sample conductivity for optimal SEM imaging.

Supplementary Text

The calculation of degree of randomness

The sequence distribution of TBT, TBS, and SBS in PBST copolyesters can be analyzed through the intensity of the corresponding peaks. **Figure S2** illustrates the three repeating units of TBT, TBS, and SBS in PBST copolyesters, with the carbon atoms in TBT and SBS exhibiting characteristic peaks ArAr and AIAI, respectively. The signal for the carbon atom in TBS is divided into peaks ArAI. The various peaks in PBST copolyesters correspond to distinct types of carbon atoms: ArAr, ArAI and AIAI. The peak intensities of the TBT, TBS, and SBS units were determined based on their respective contents, using equations similar to those reported in the literature. The calculated average sequence lengths of the BT and BS units (L_{BT} and L_{BS}) and the degree of randomness (R) are presented in Table S2, derived from the ^{1}H NMR spectra using the following **Equation S4-9**.

$$N_{TBT} = I_{ArAr} / (I_{ArAr} + I_{ArAI} + I_{AIAI}) \quad \textbf{(Equation S4)}$$

$$N_{TBS} = I_{ArAI} / (I_{ArAr} + I_{ArAI} + I_{AIAI}) \quad \textbf{(Equation S5)}$$

$$N_{SBS} = I_{AIAI} / (I_{ArAr} + I_{ArAI} + I_{AIAI}) \quad \textbf{(Equation S6)}$$

$$L_{BT} = 1 + 2\, I_{ArAr} / I_{ArAI} \quad \textbf{(Equation S7)}$$

$$L_{BS} = 1 + 2\, I_{AIAI} / I_{ArAI} \quad \textbf{(Equation S8)}$$

$$R = 1 / L_{BT} + 1 / L_{BS} \quad \textbf{(Equation S9)}$$

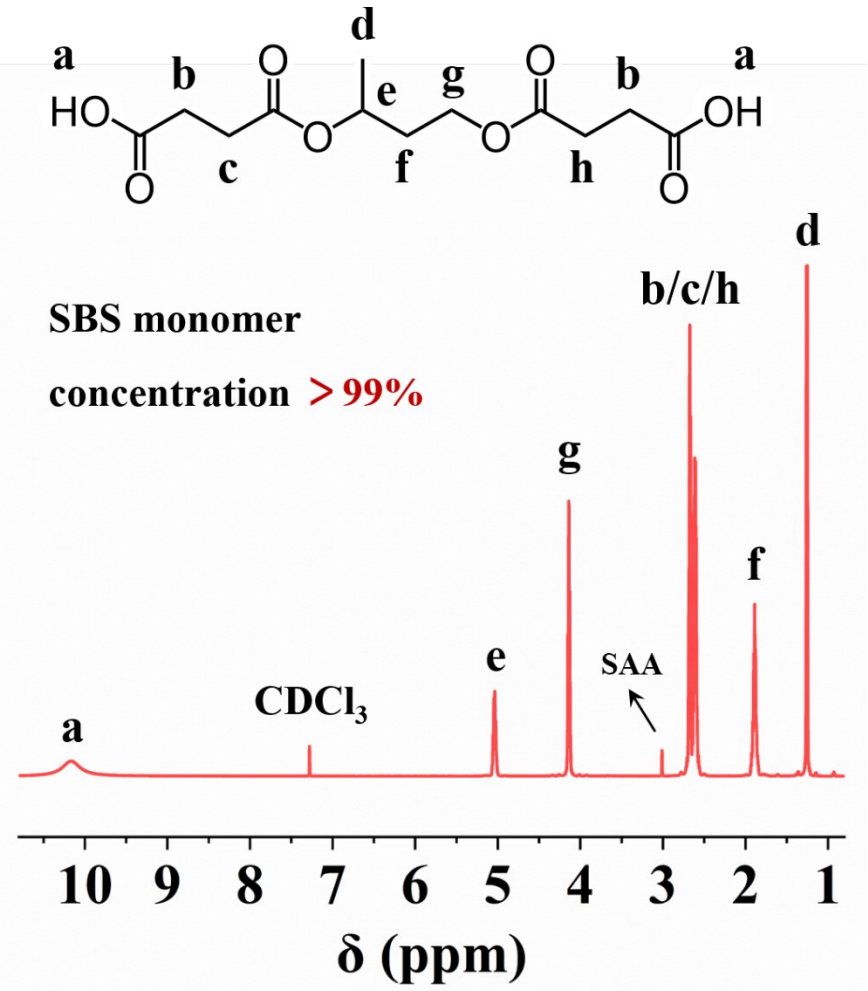

Fig. S1 ^{1}H NMR spectra of SBS Monomer.

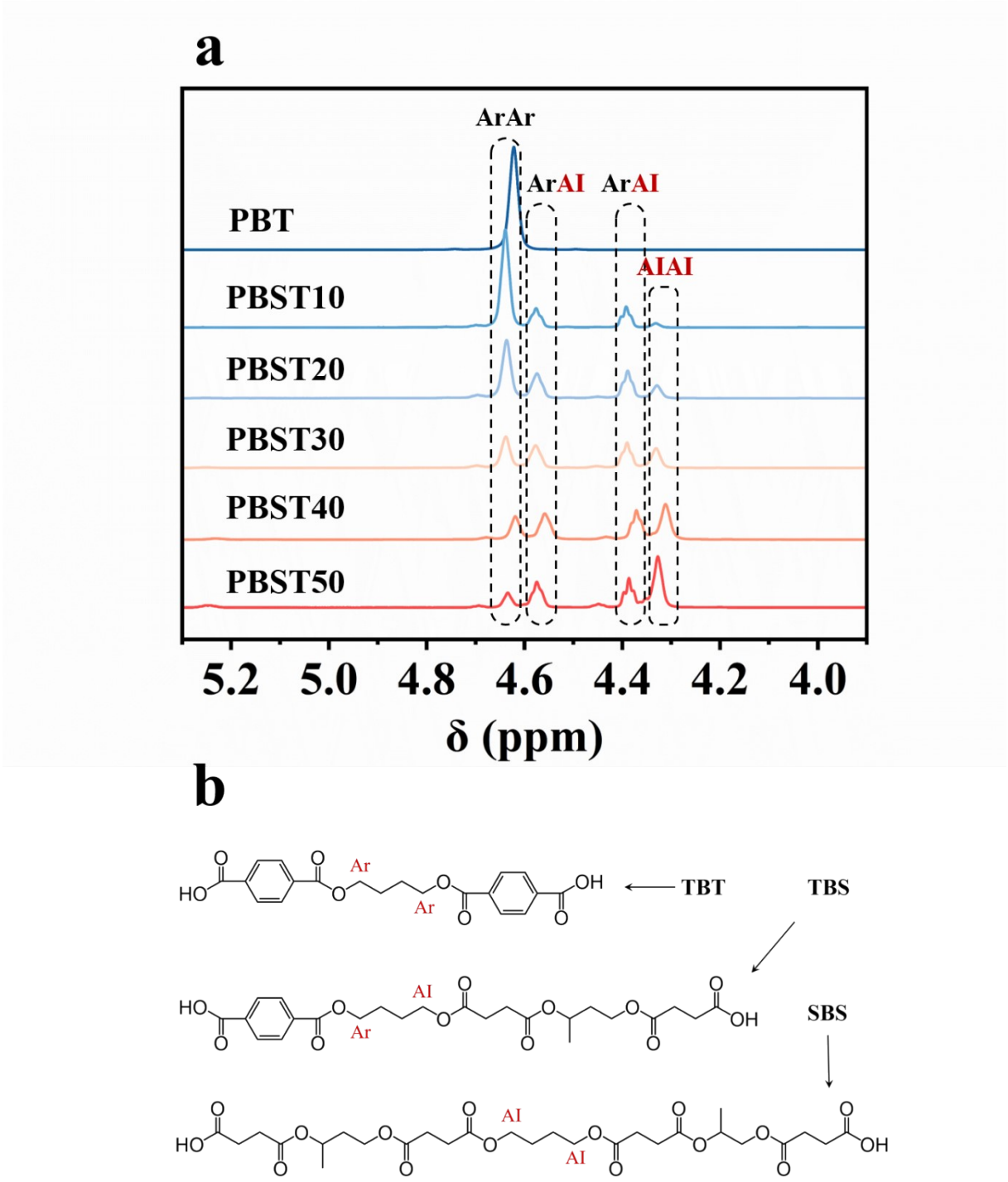

Fig. S2 ^{1}H NMR spectra of sequence structure of triads (a), and the sequence structure of triads in the PBST copolyesters (b).

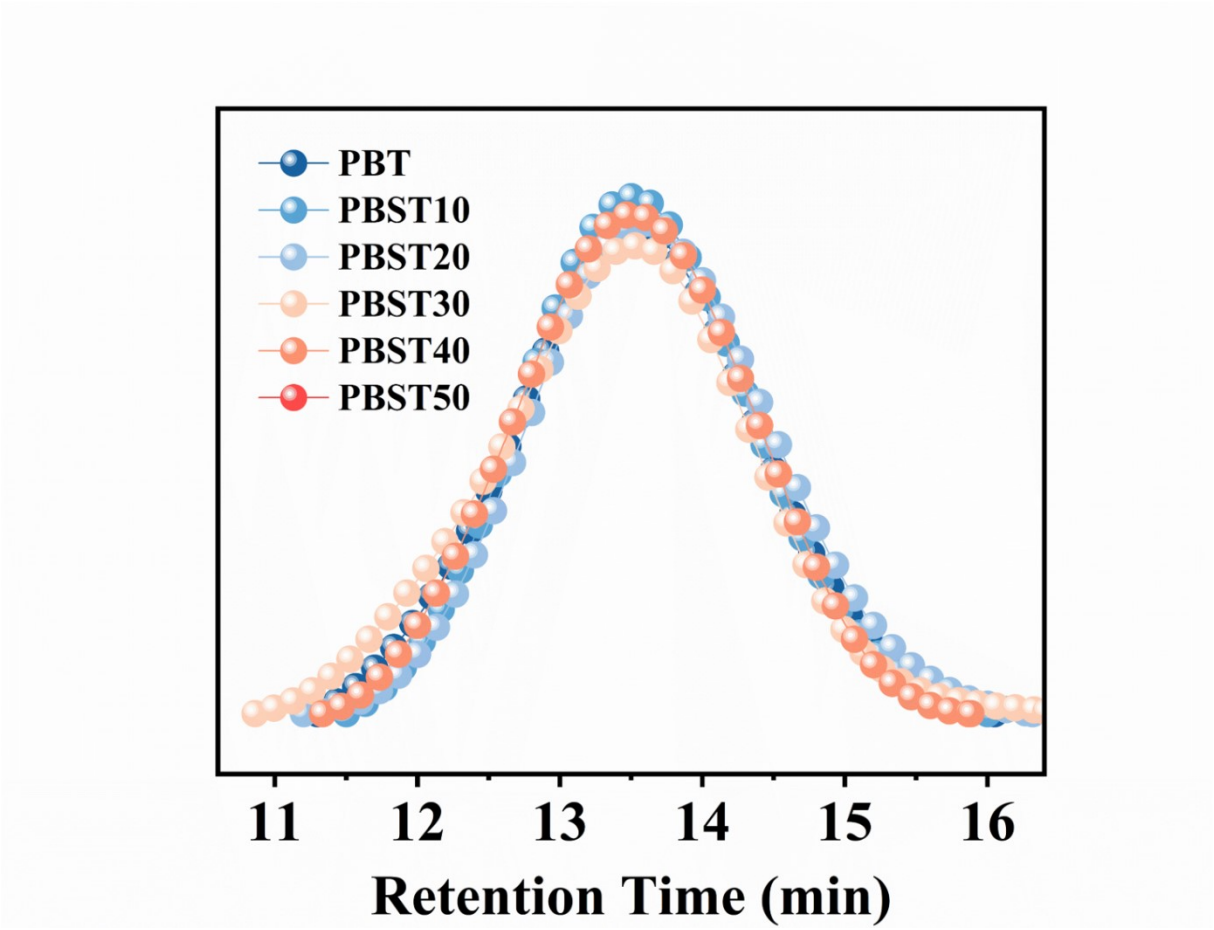

Fig. S3 GPC profiles of the PBST copolyesters.

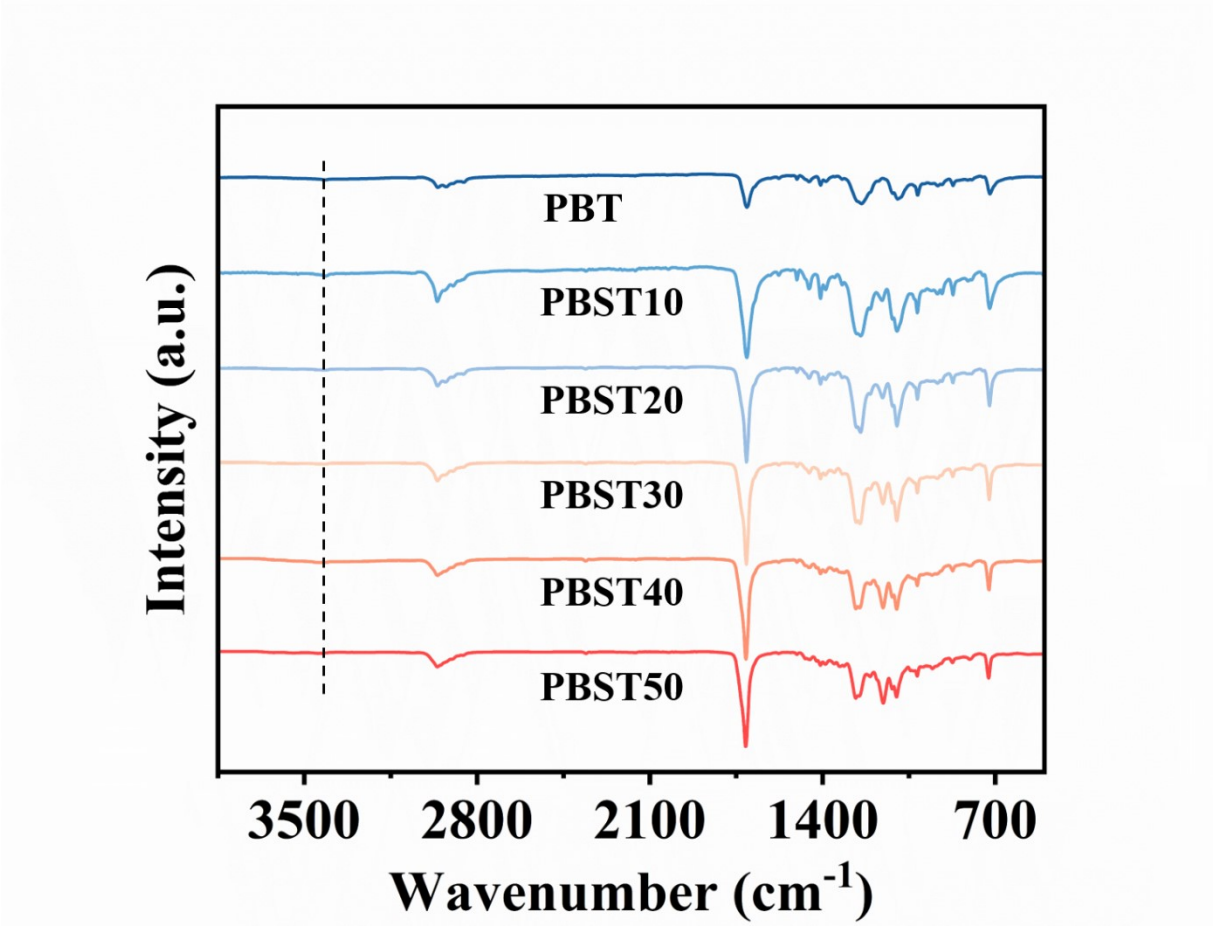

Fig. S4 FTIR Measurement of PBST Copolyesters.

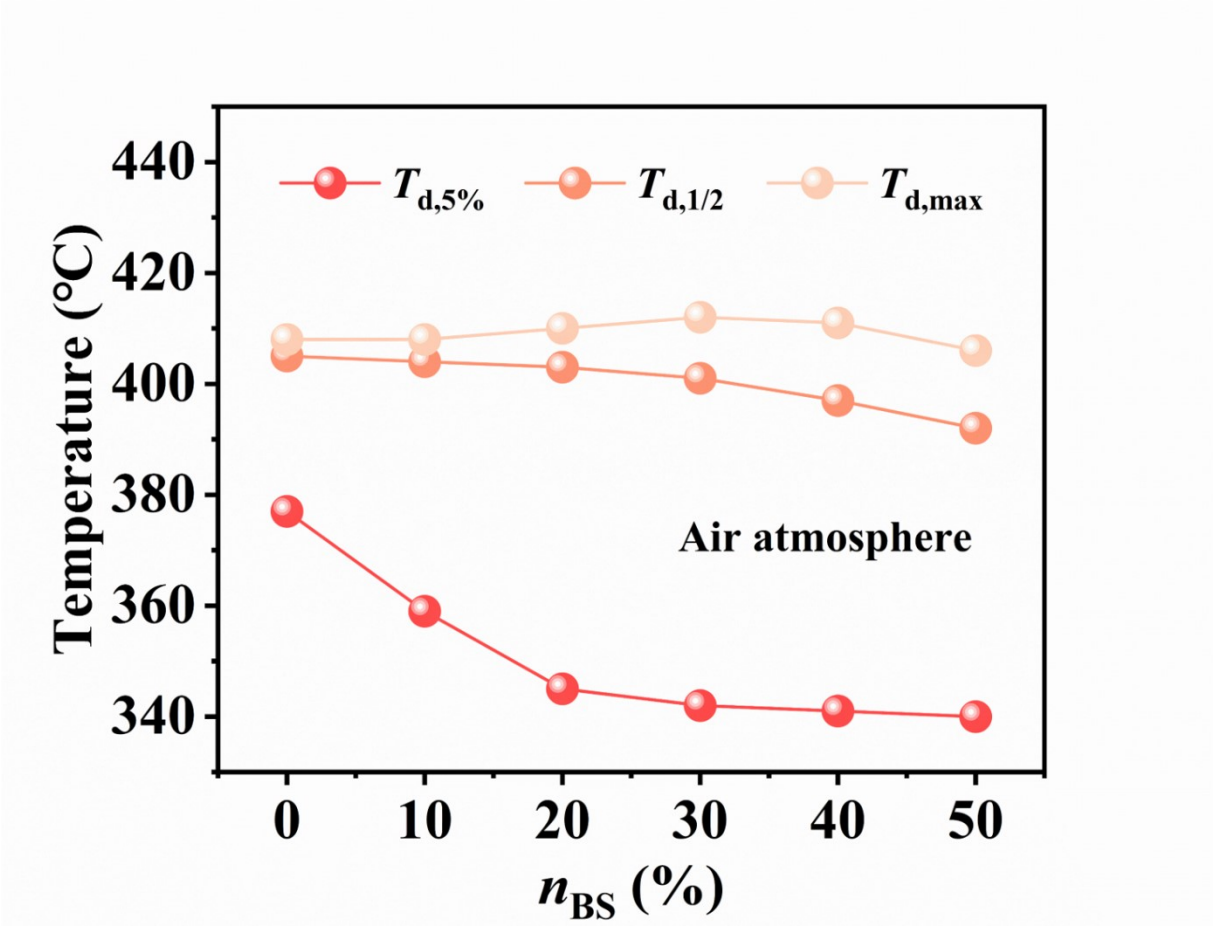

Fig. S5 variation trends of $T_{d,5\%}$, $T_{d,1/2}$, and $T_{d,max}$ for PBST copolyesters with various components in air atmosphere.

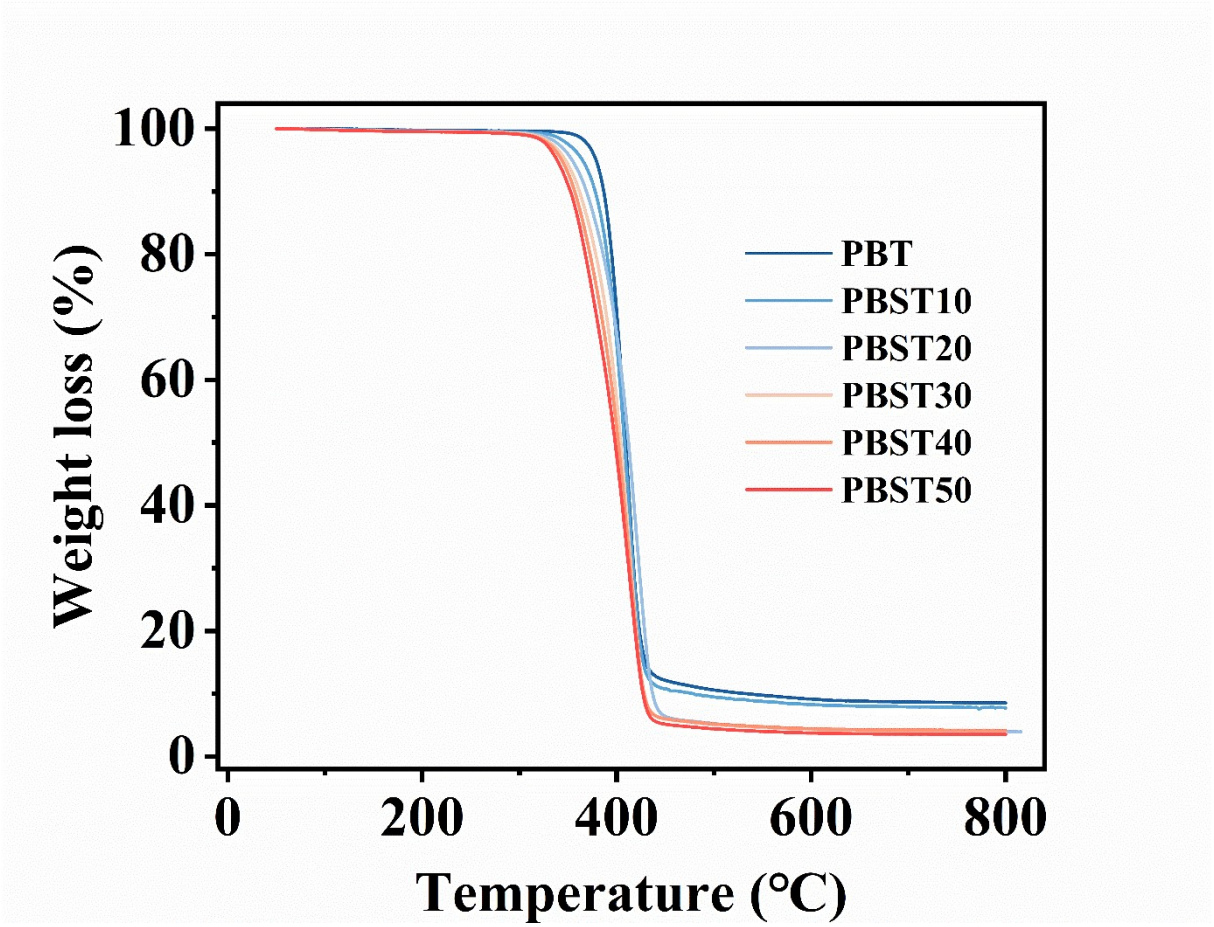

Fig. S6 TGA curves of PBST copolyesters in N_2 atmosphere.

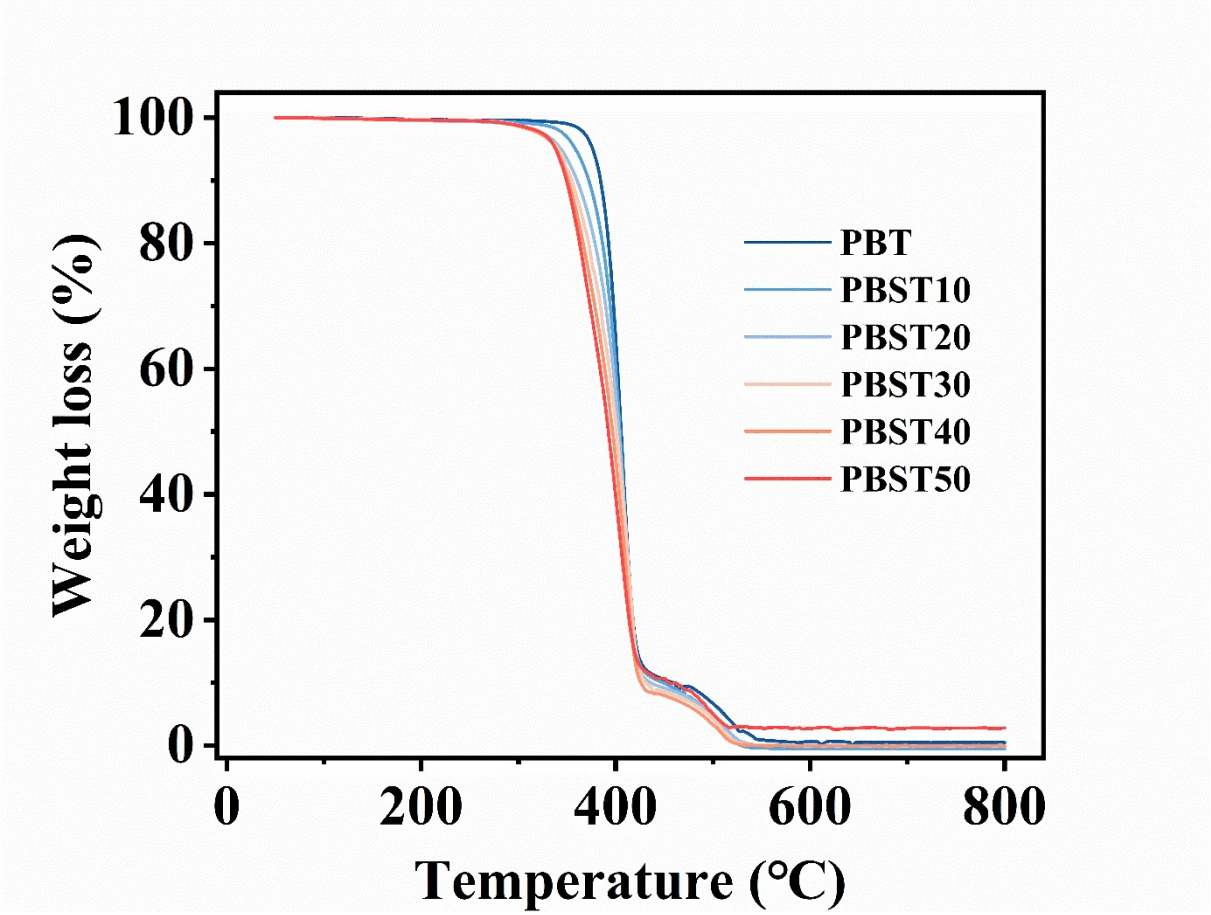

Fig. S7 TGA curves of PBST copolyesters in air atmosphere.

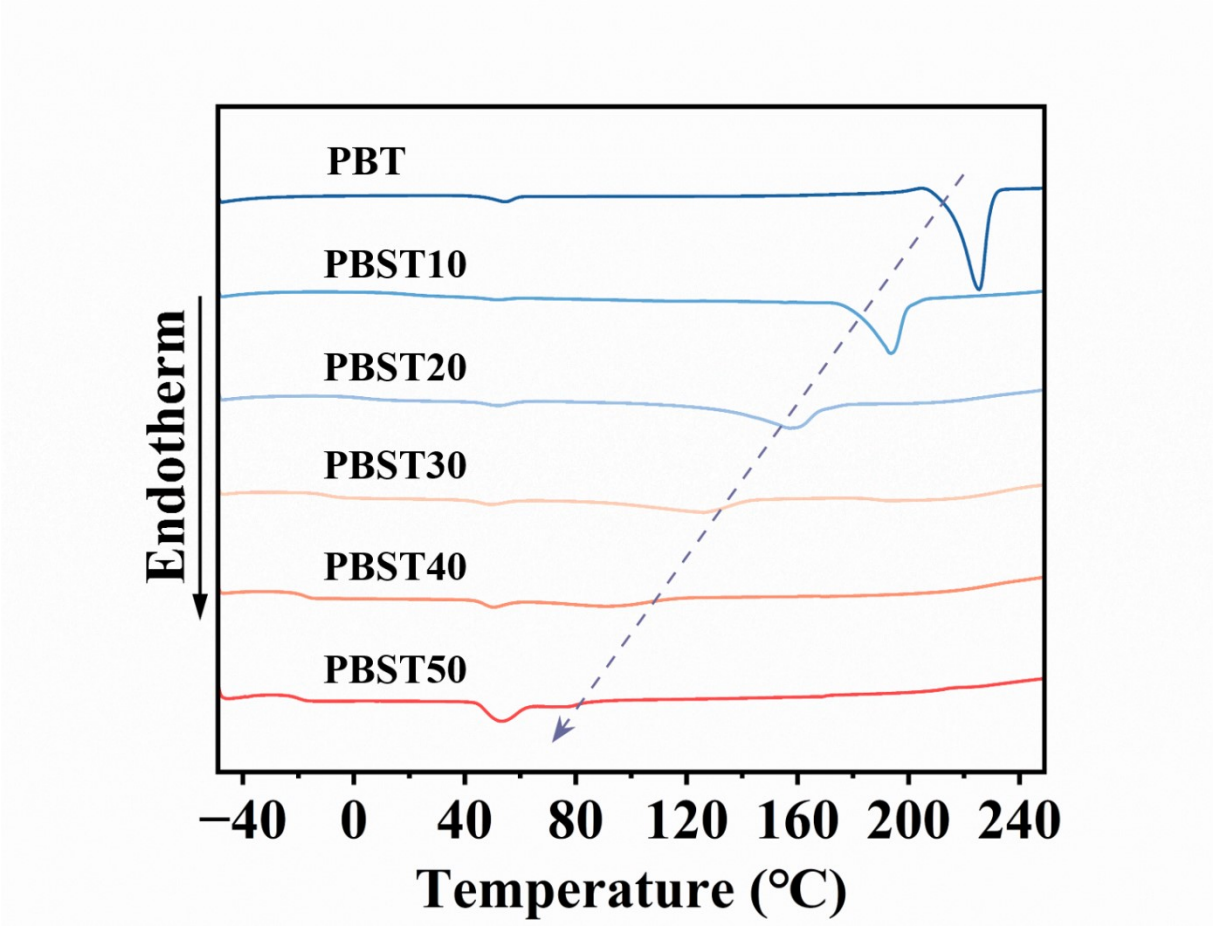

Fig. S8 The melting enthalpies of PECS copolyesters after crystallizing for various times calculated by DSC curves.

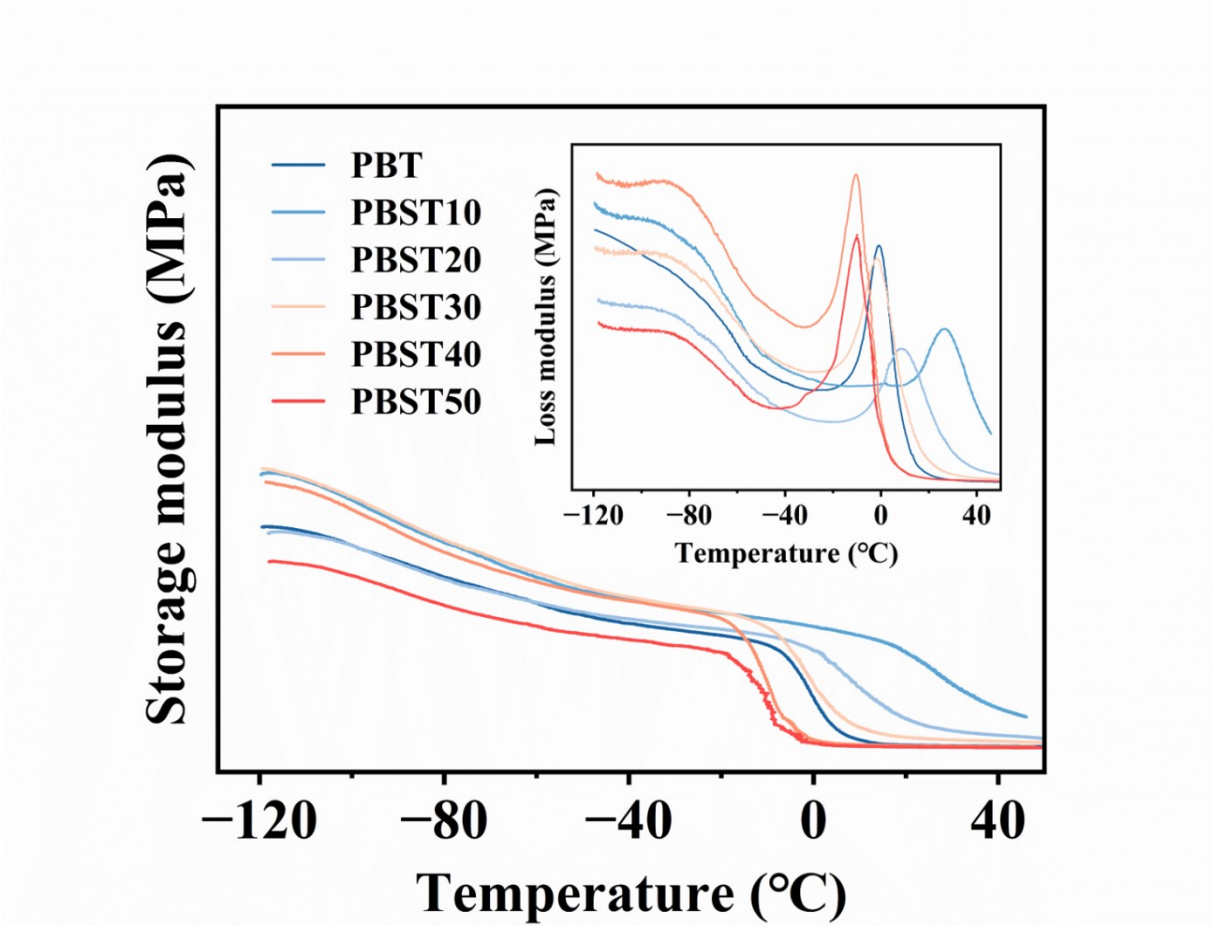

Fig. S9 Storage and loss modulus of PBST copolyesters determined by DMA.

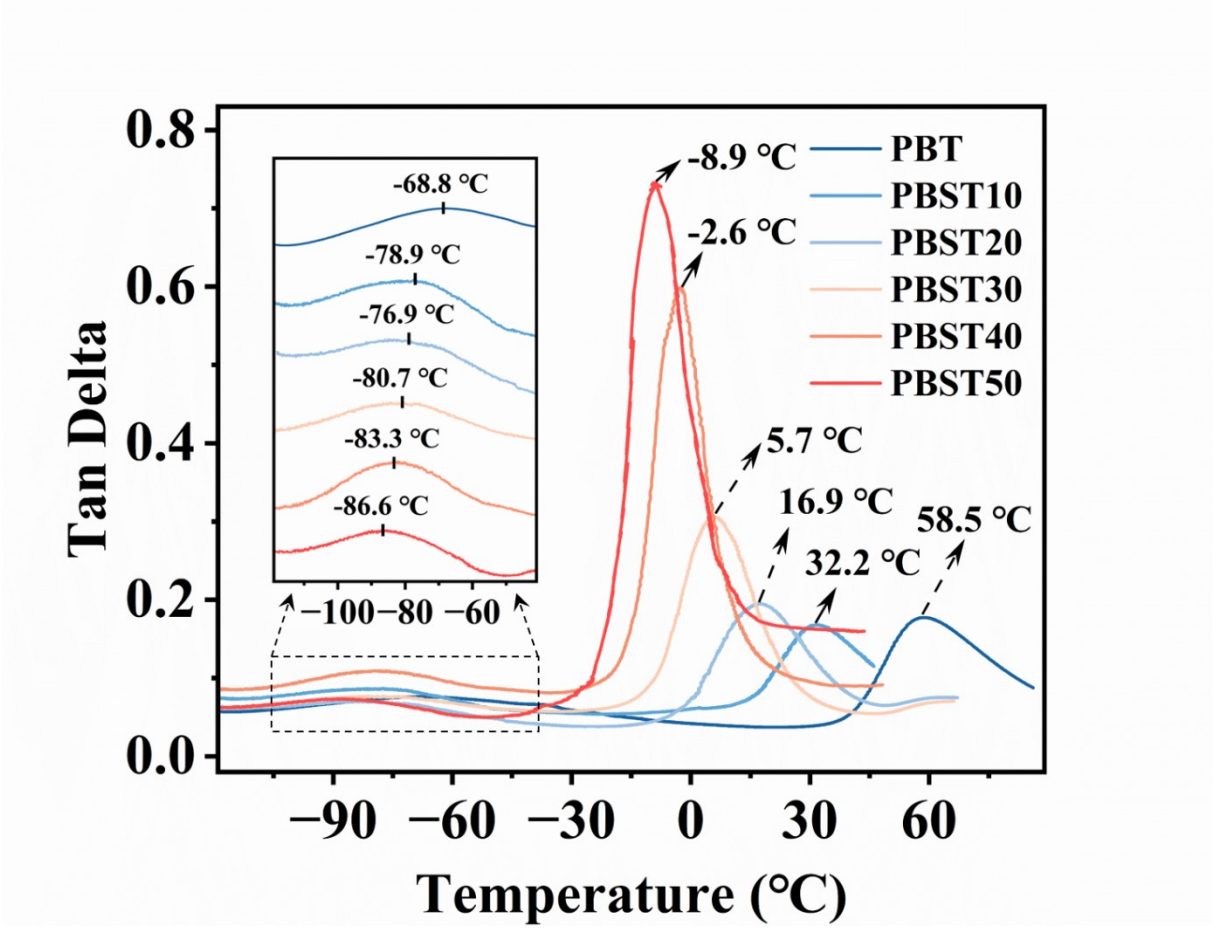

Fig. S10 The tan delta as a function of temperature for PBST copolyesters.

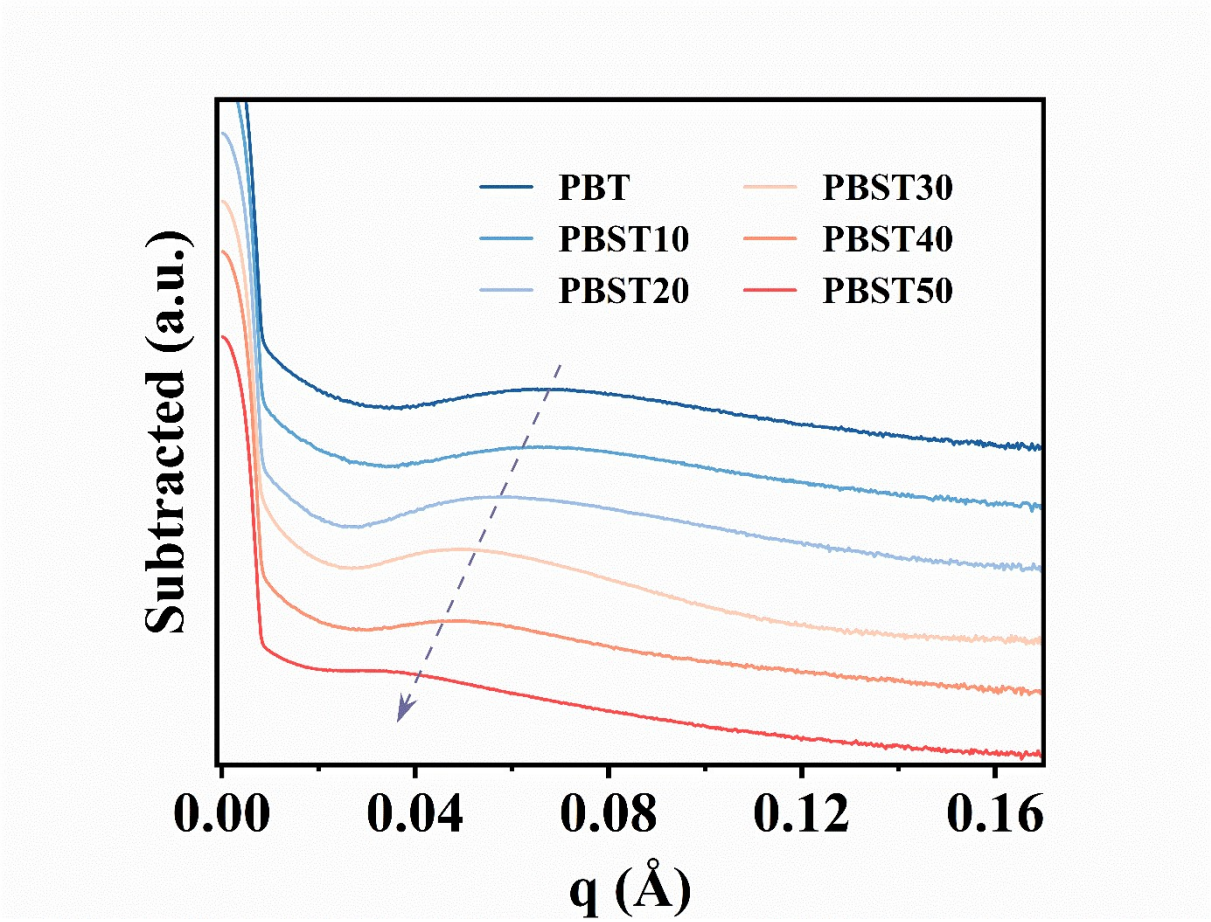

Fig. S11 The SAXS One-Dimensional Curve for PBST copolyesters.

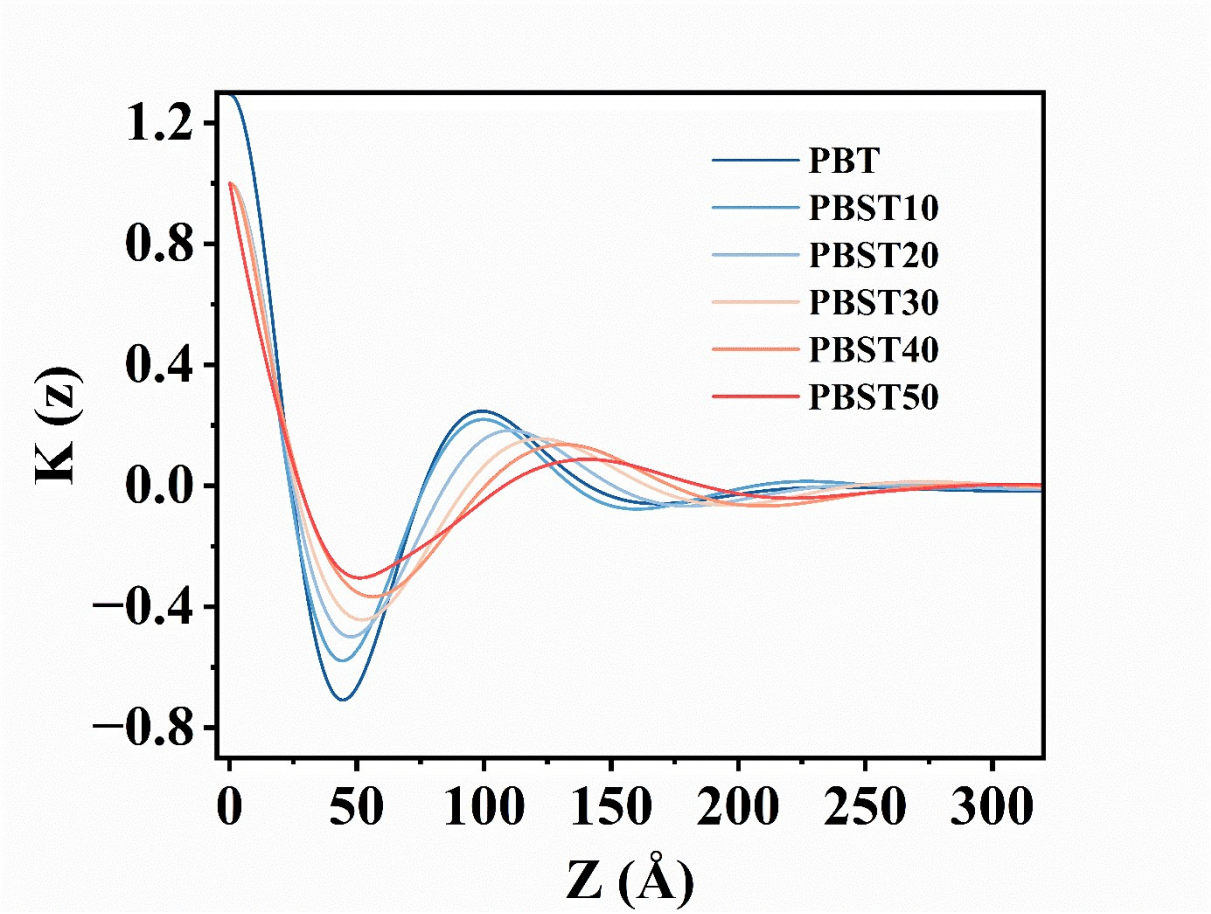

Fig. S12 One-dimensional electron density correlation function of PBST copolyesters.

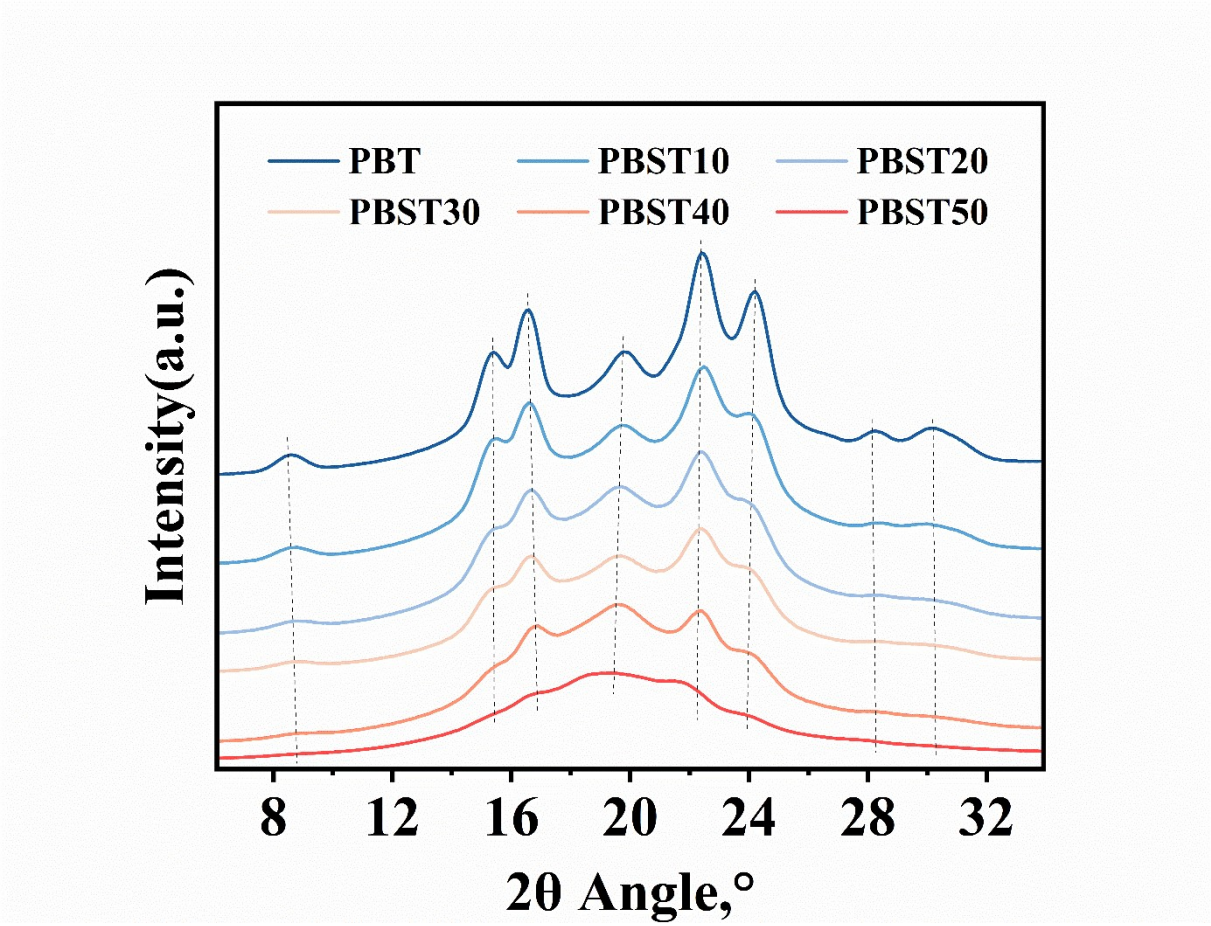

Fig. S13 The WAXS One-Dimensional Curve for PBST copolyesters.

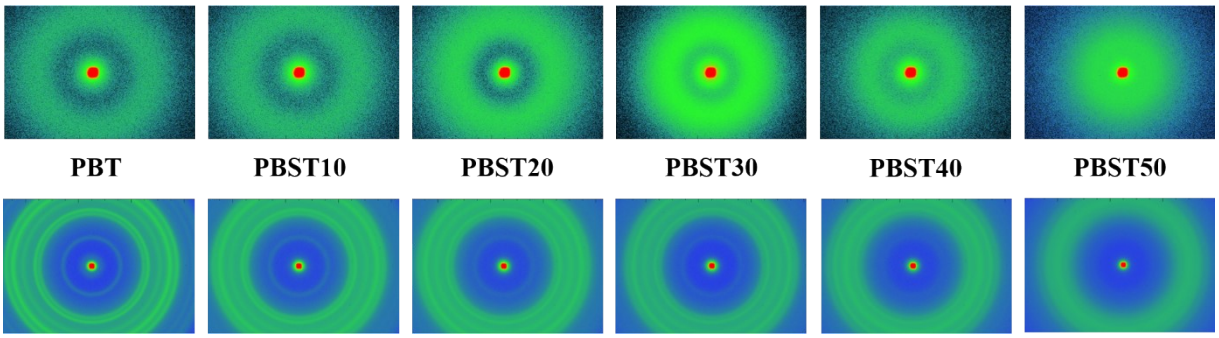

Fig. S14 2D patterns of SAXS and WAXS of PBST copolyesters.

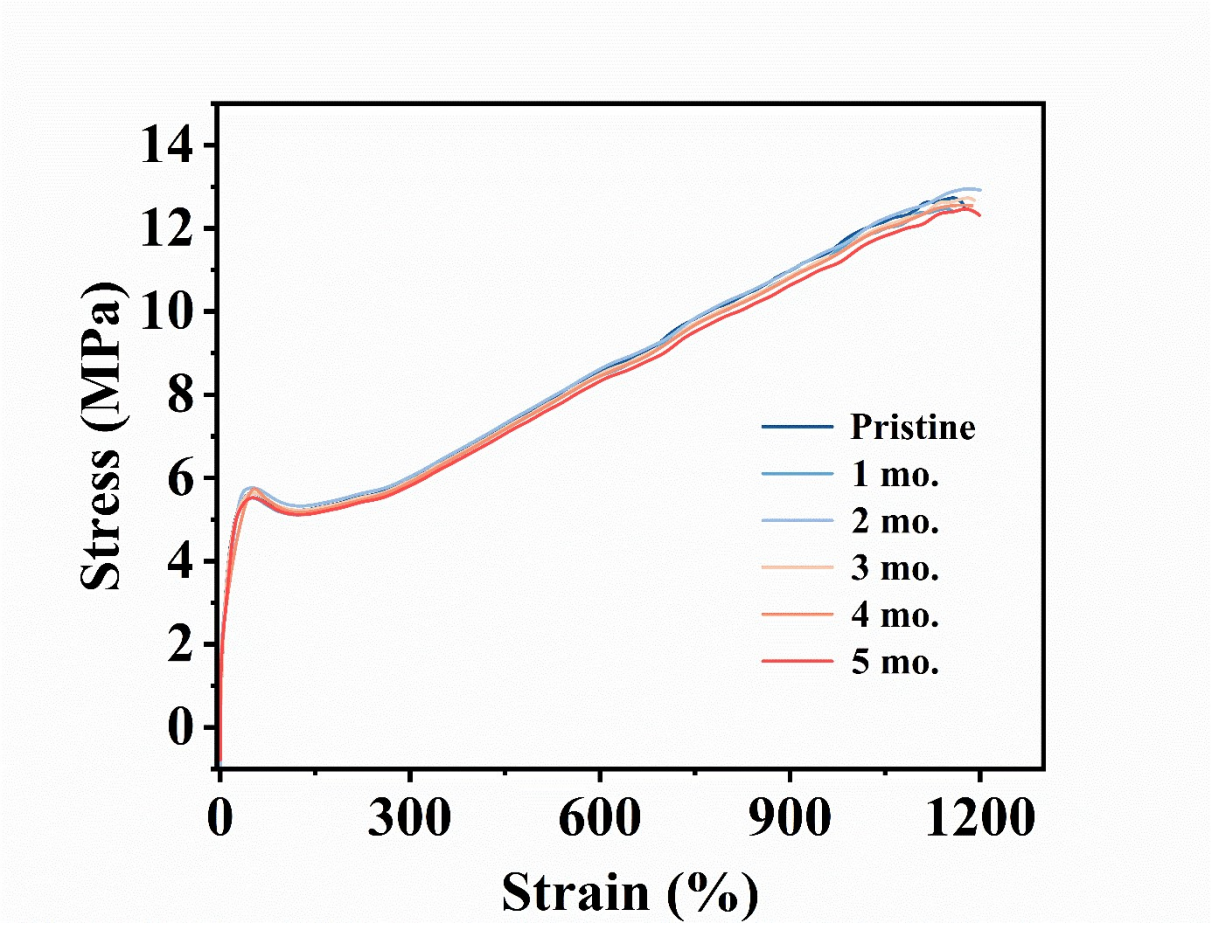

Fig. S15 Stress-Strain Curves of PBST Copolyesters Under Different Storage Times.

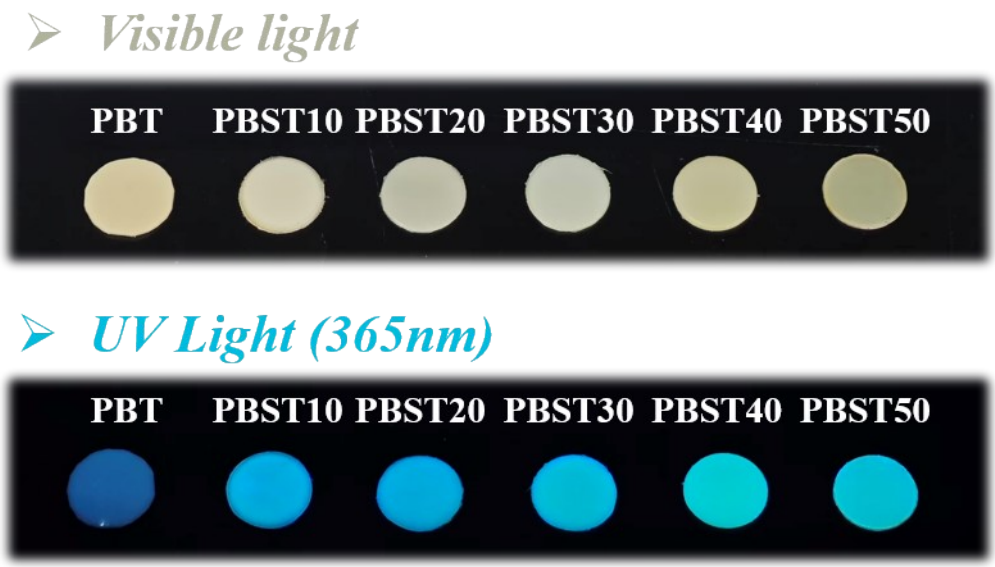

Fig. S16 images under visible light and ultraviolet (UV) light of PBST copolyesters.

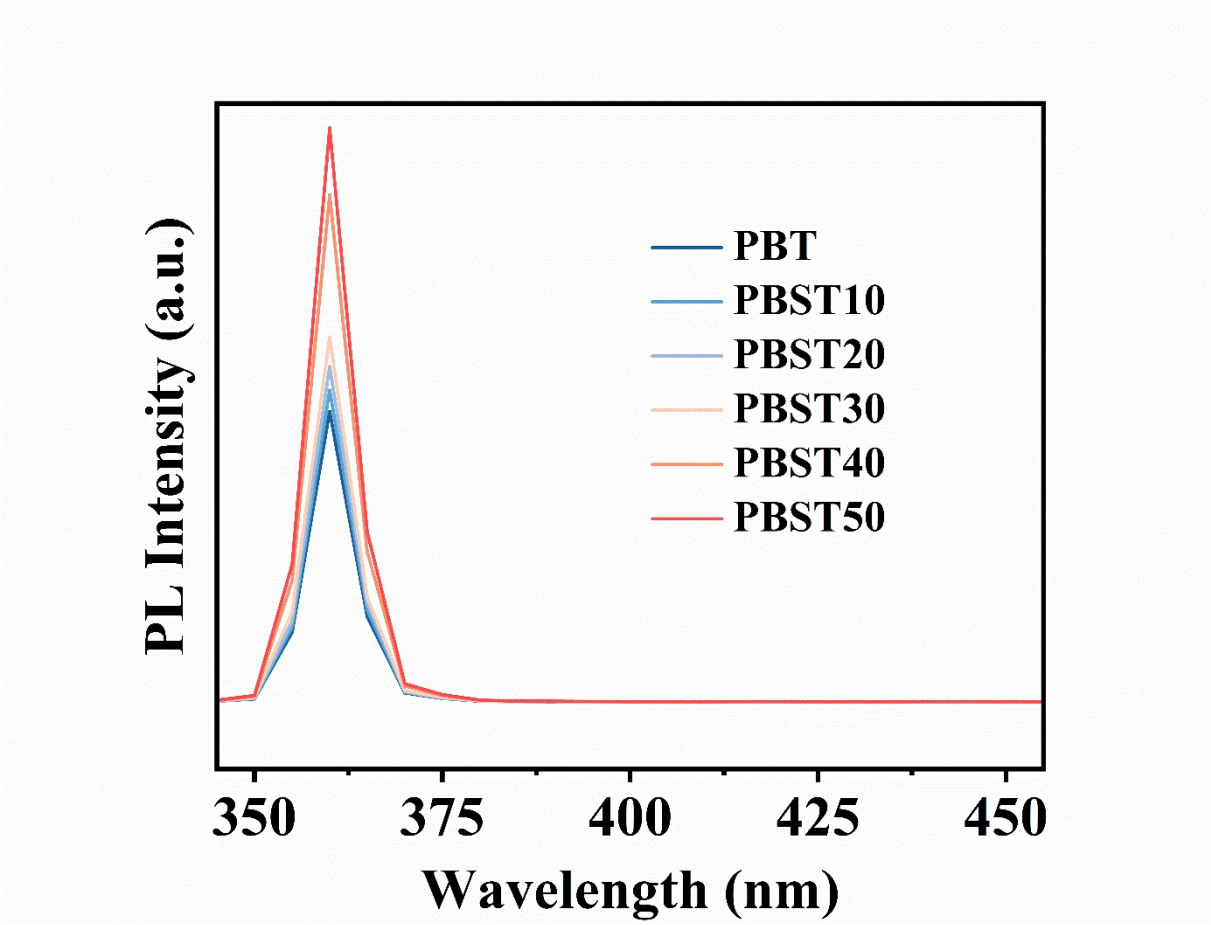

Fig. S17 Fluorescence quantum yields of PBST copolyesters.

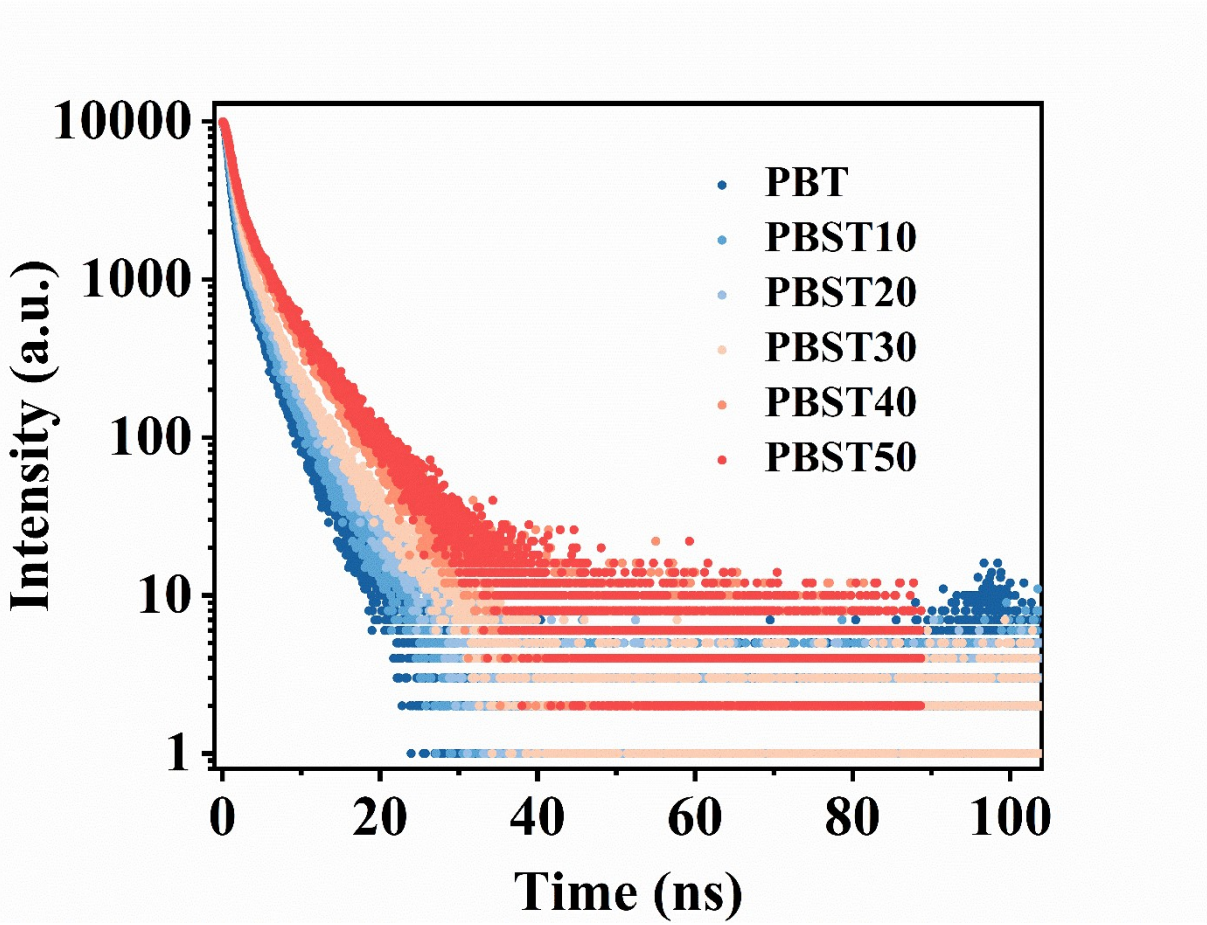

Fig. S18 Fluorescence lifetimes of solutions of PBST copolyesters (solvent: DMSO).

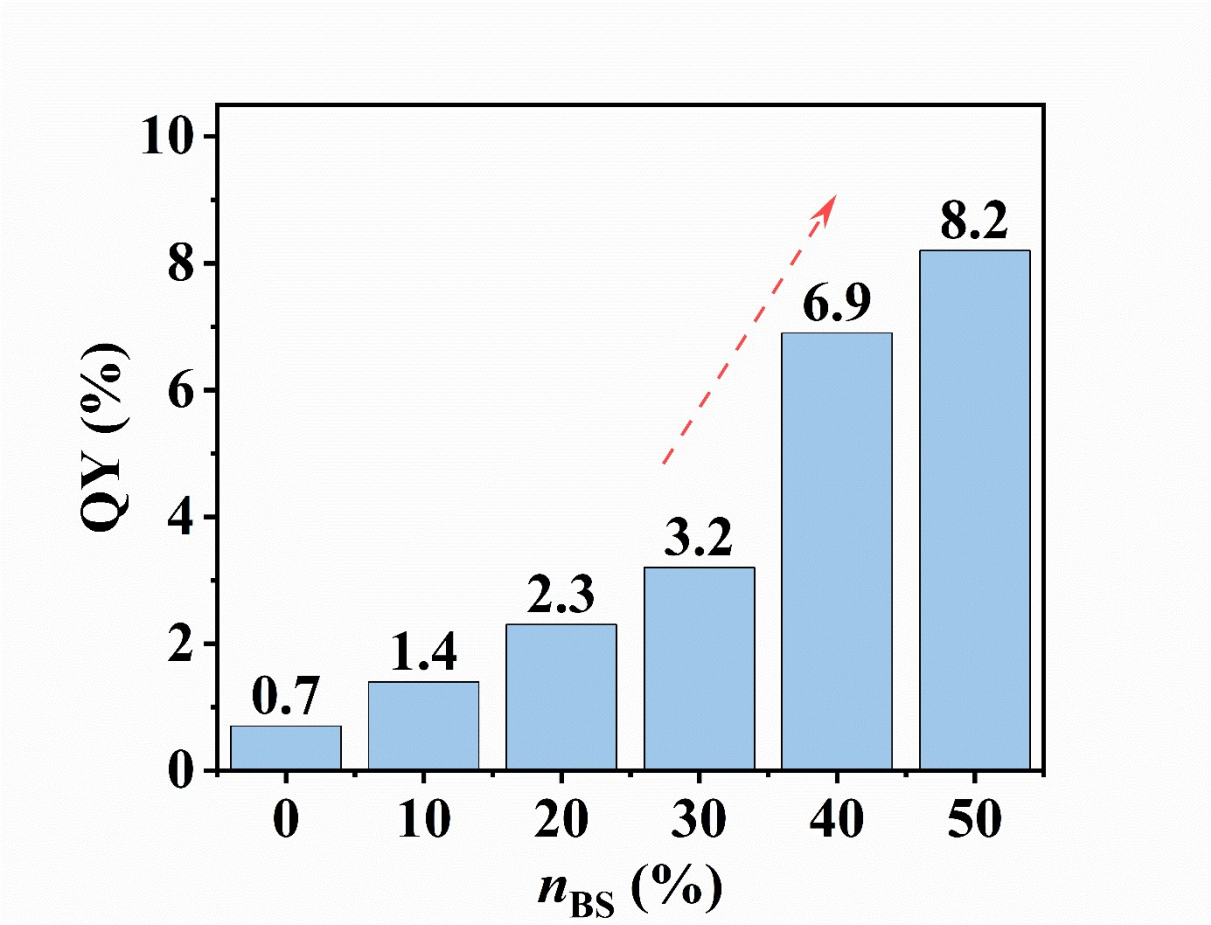

Fig. S19 Fluorescence quantum yield (QY) as a function of n_{BS} of PBST copolyesters.

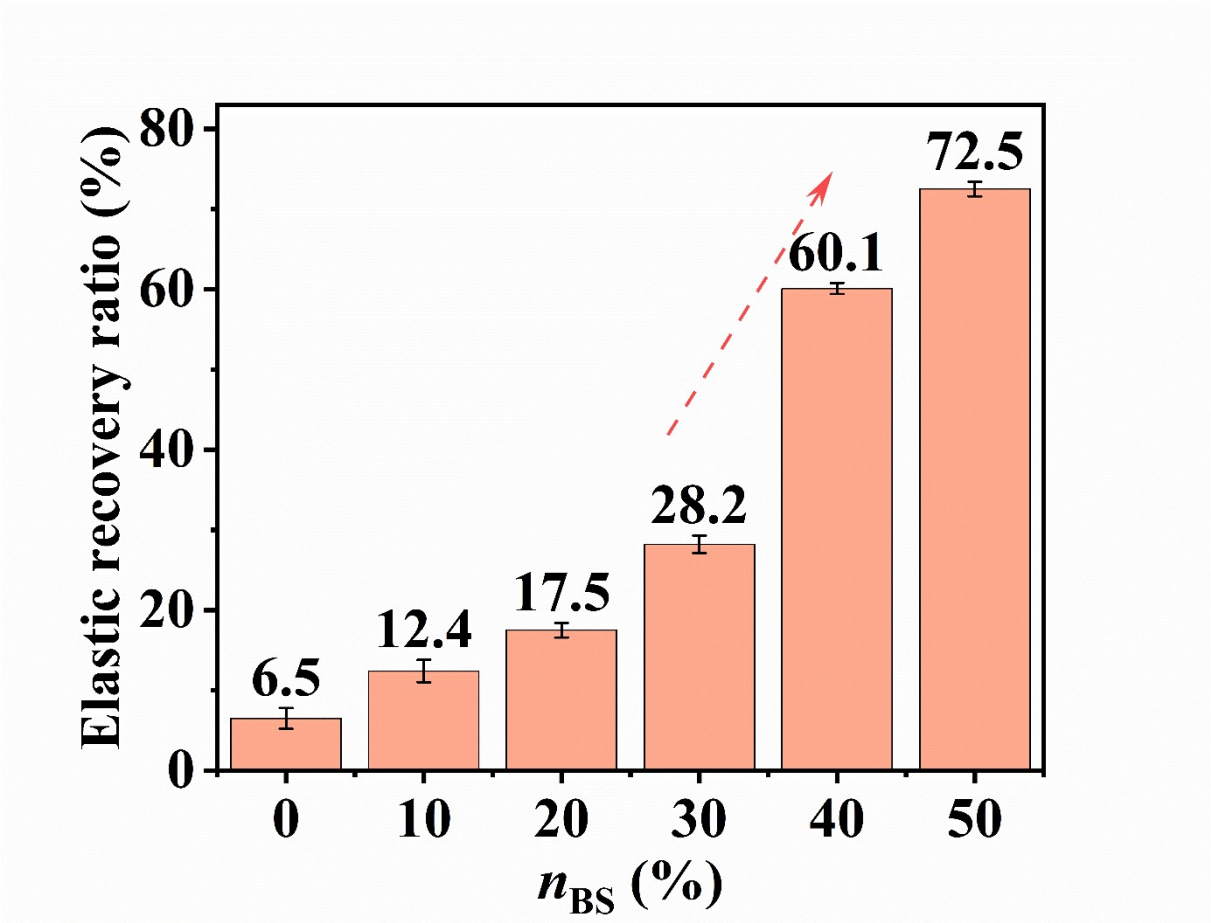

Fig. S20 Elastic recovery ratio as a function of n_{BS} of PBST copolyesters.

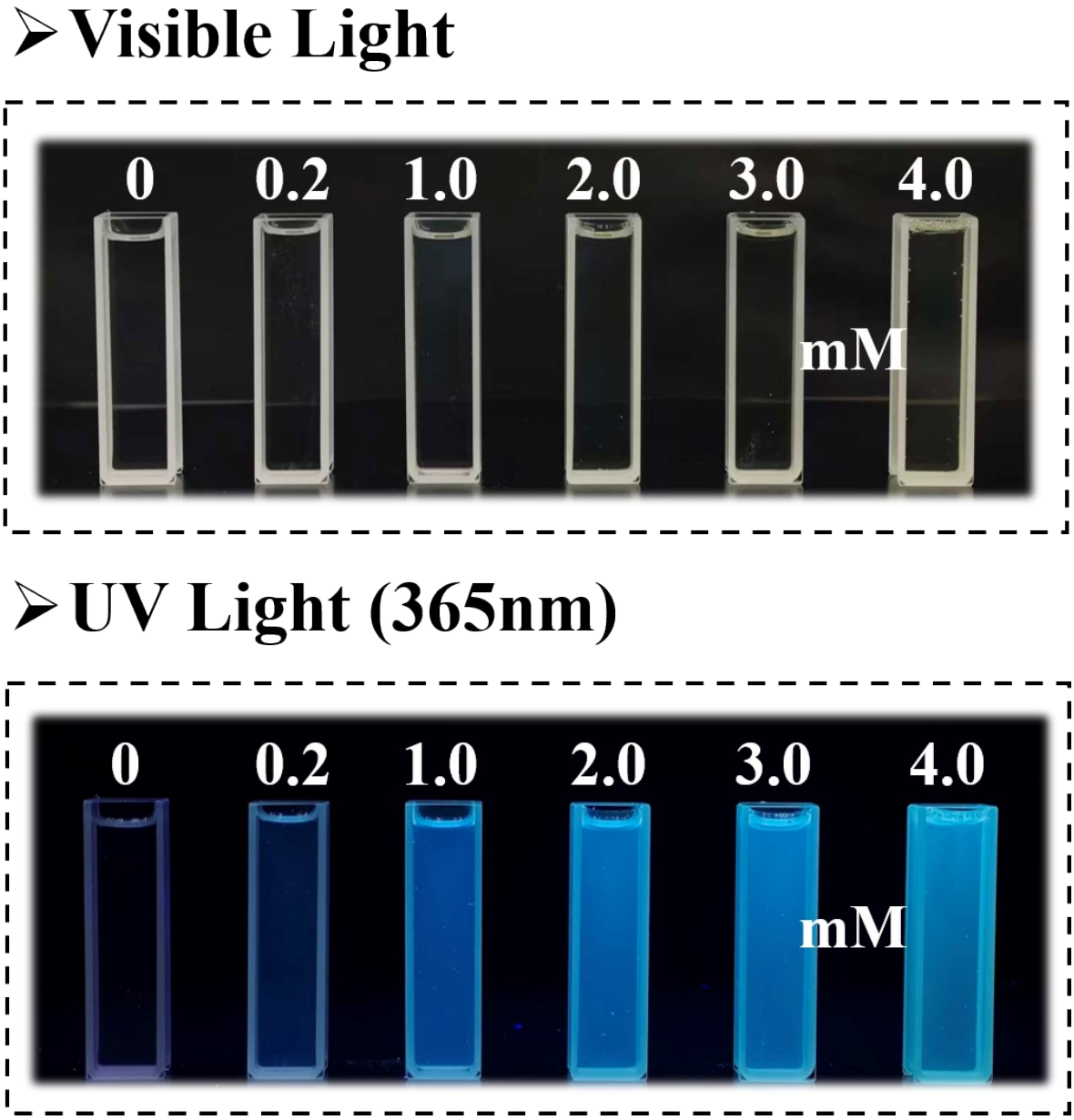

Fig. S21 images under visible light and ultraviolet (UV) light of PBST40 solutions with different concentrations (solvent: $CDCl_3$).

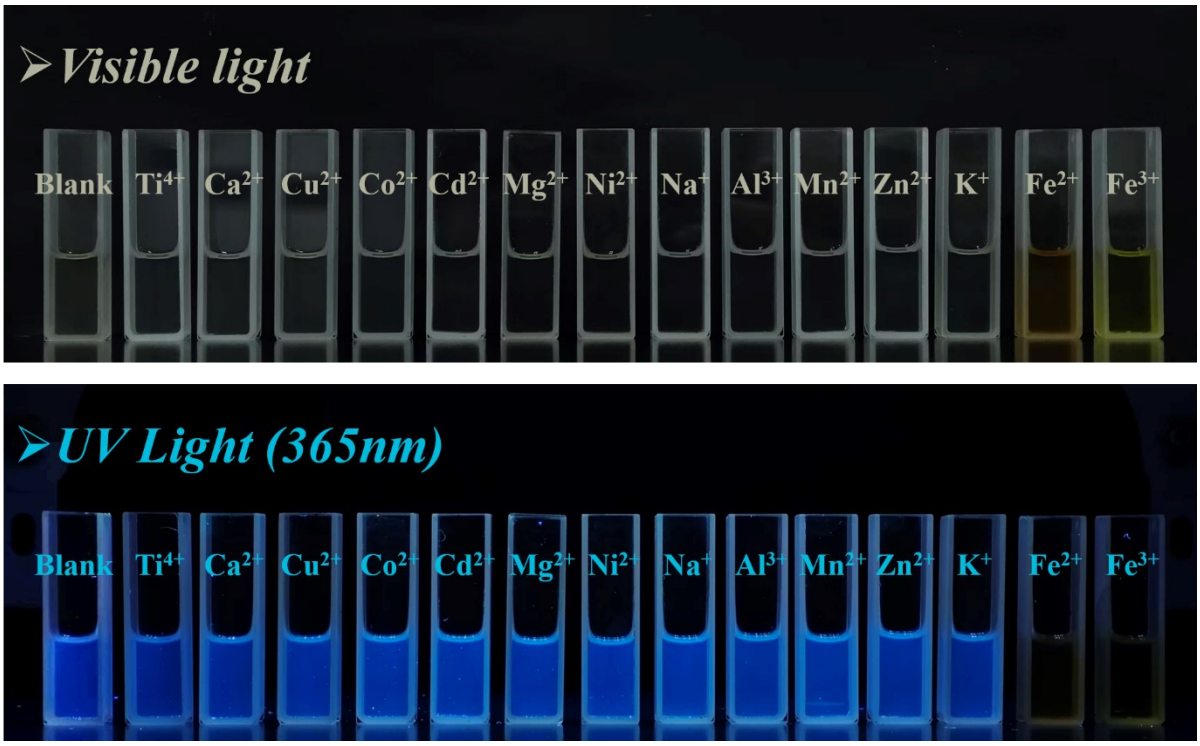

Fig. S22 Images under visible light and UV light of PBST40 solutions (solvent: DMSO) after adding different metal ions.

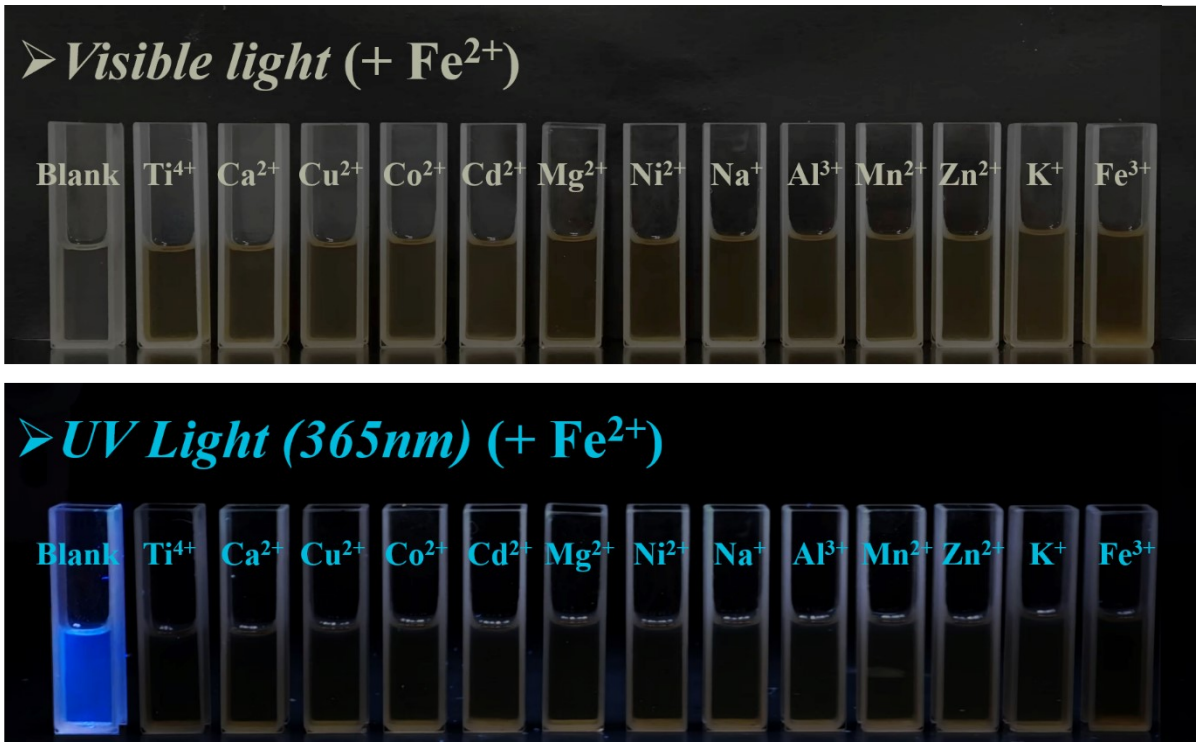

Fig. S23 Images under visible light and UV light of PBST40 solutions (solvent: DMSO) after adding Fe^{2+} in the presence of a second metal ion.

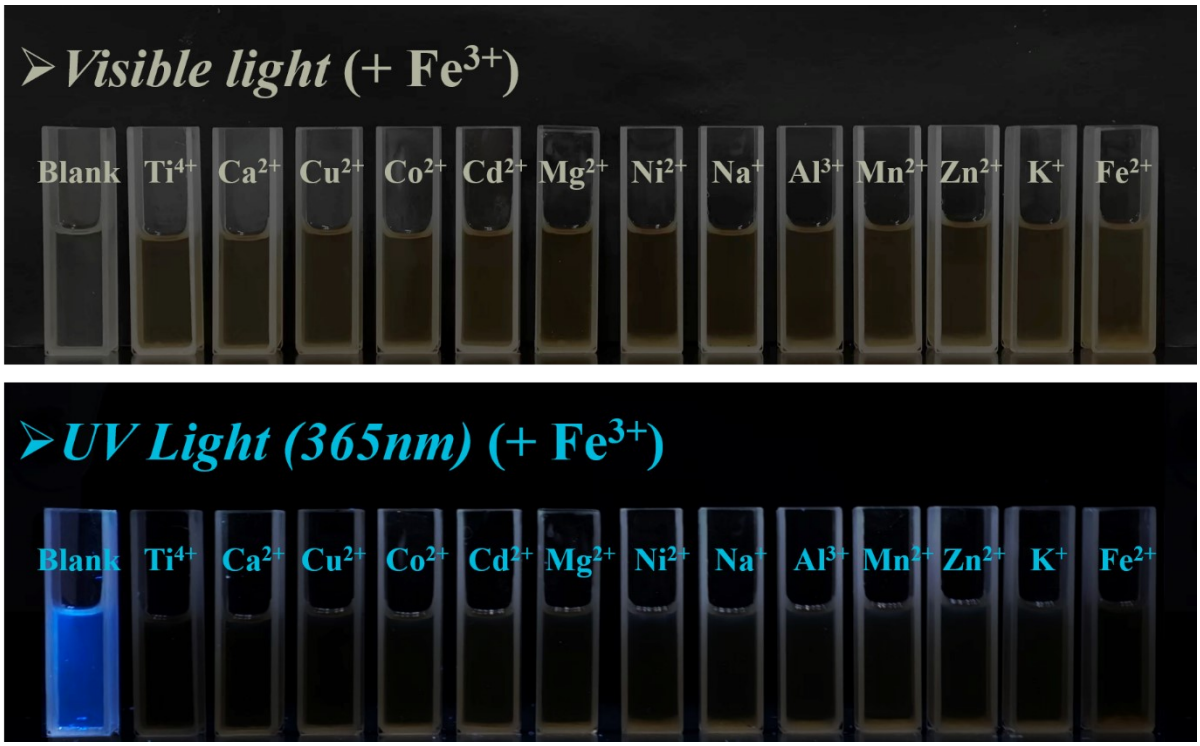

Fig. S24 Images under visible light and UV light of PBST40 solutions (solvent: DMSO) after adding Fe^{3+} in the presence of a second metal ion.

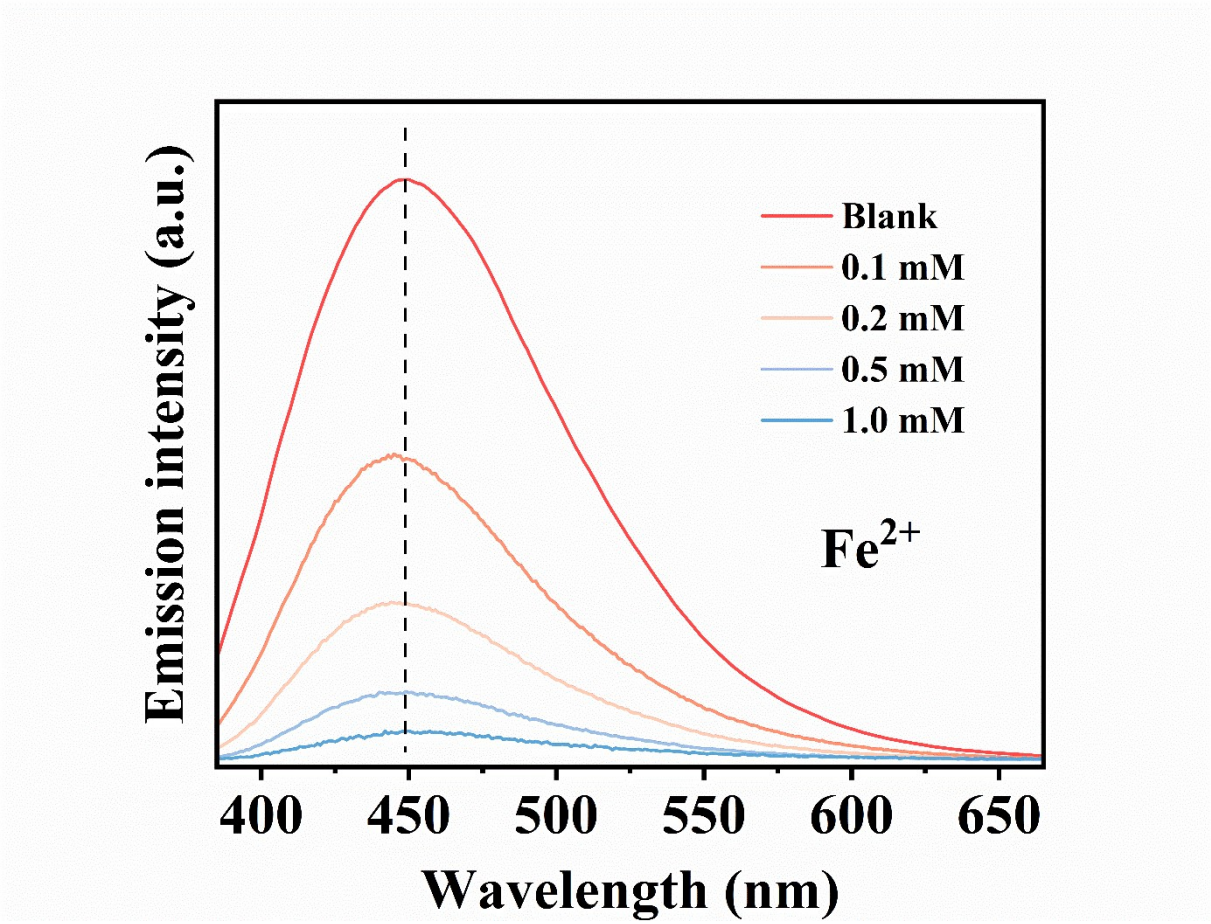

Fig. S25 Fluorescence emission spectra of PBST40 solution with different Fe^{2+} concentrations.

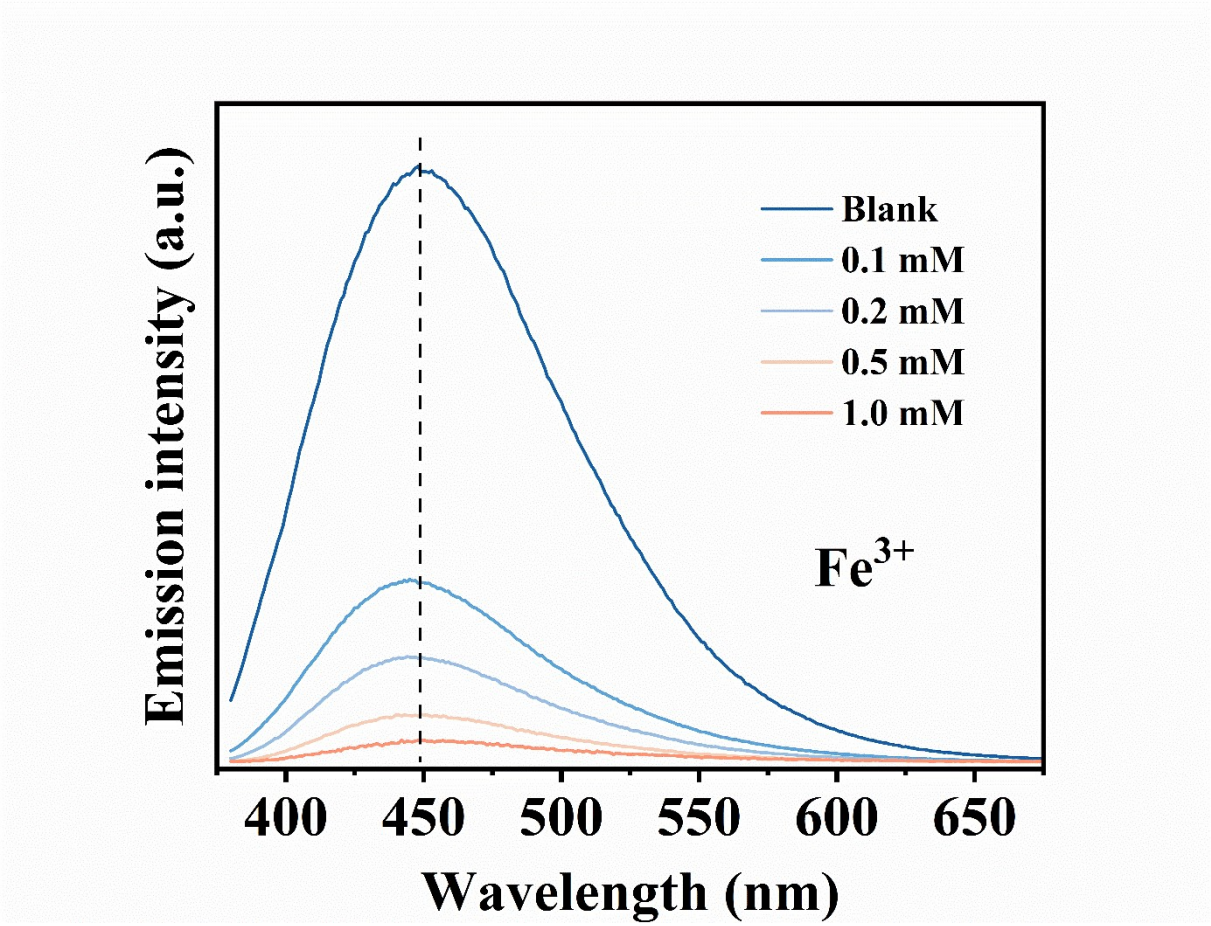

Fig. S26 Fluorescence emission spectra of PBST40 solution with different Fe^{3+} concentrations.

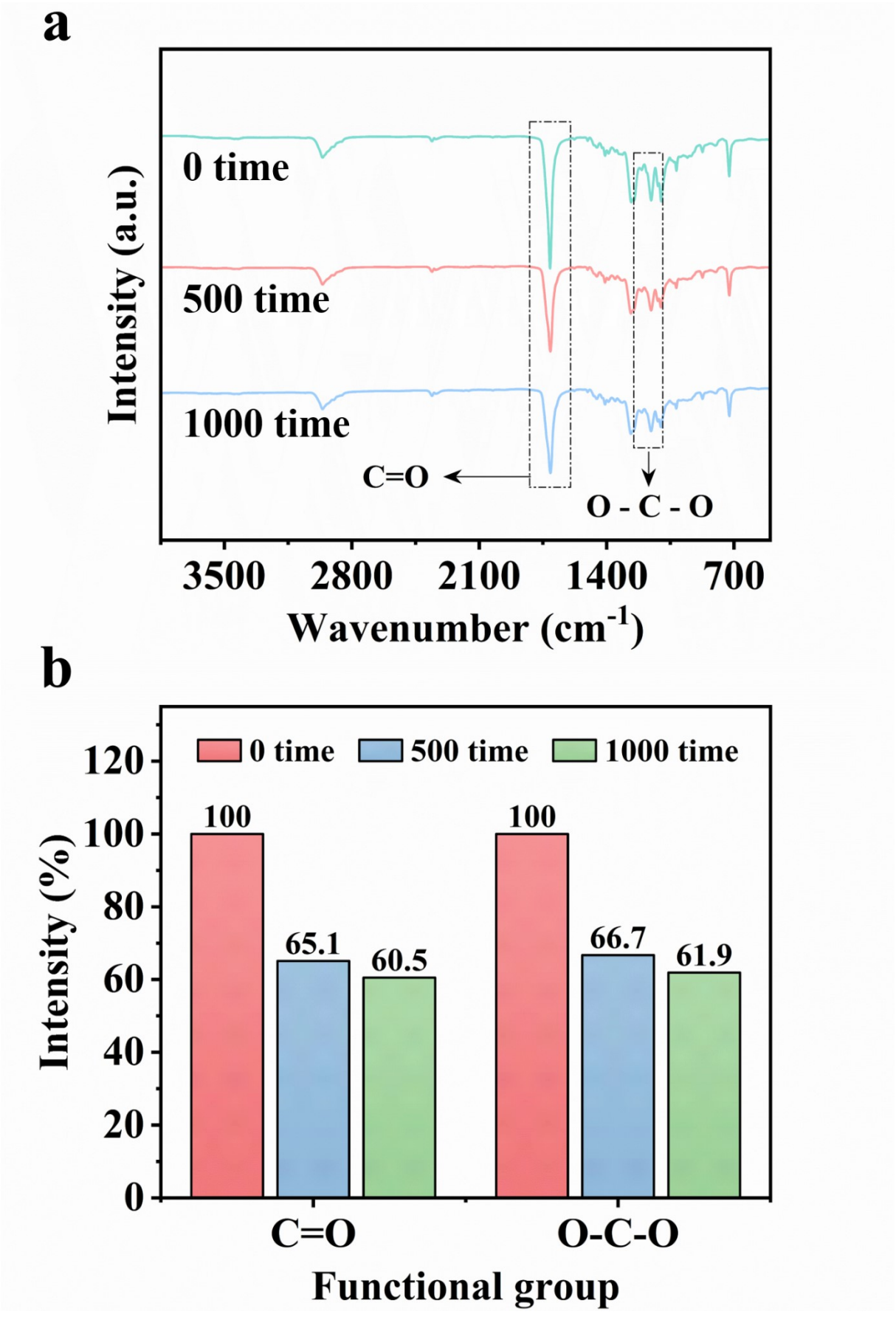

Fig. S27 (a)FT-IR spectra, and (b)The intensity changes of C=O and O-C-O under different cycle numbers of PBST40.

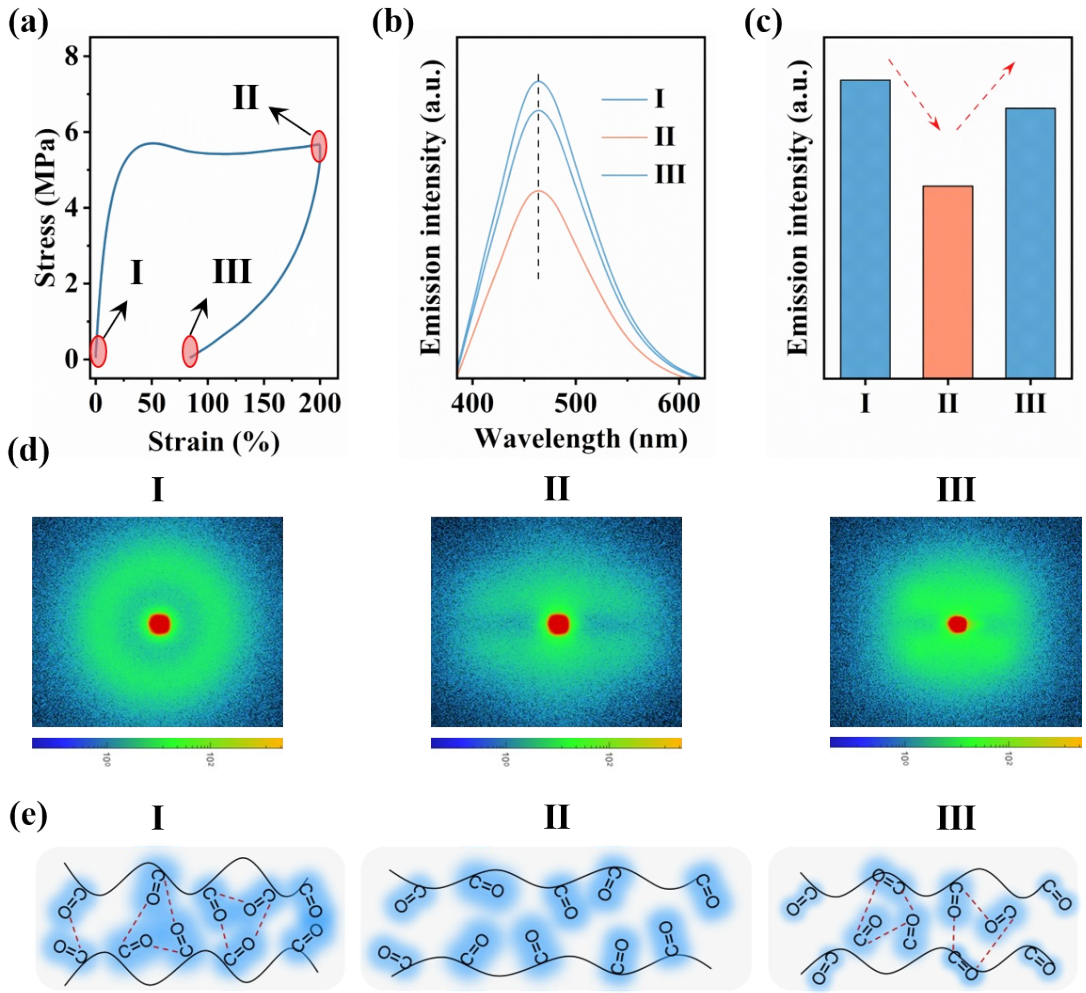

Fig. S28 (a) Cyclic loading-unloading stress curves of PBST40, (b-c) fluorescence intensity, (d) 2D SAXS patterns, and (e) molecular chain conformations and cluster formation at different strains.

Table S1. Feeding ratio, GPC tests, and the content of BS chain segment in PBST copolyesters

Sample	Feeding (mol)			GPC[a]			$[\eta]^b$	BS mol.% in the final products [c]
	1,4-BDO	DMT	SBS	M_n (g/mol)	M_w (g/mol)	$Đ$		
PBT	0.56	0.40	0	40 000	59 000	1.47	1.12	0
PBST10	0.52	0.40	0.04	49 000	86 000	1.75	1.15	10
PBST20	0.48	0.40	0.08	50 000	88 000	1.77	1.16	20
PBST30	0.44	0.40	0.12	52 000	96 000	1.85	1.18	30
PBST40	0.40	0.40	0.16	53 000	95 900	1.81	1.19	40
PBST50	0.36	0.40	0.20	54 000	95 000	1.76	1.21	50

[a] Determined by GPC in $CHCl_3$ calibrated with standard polystyrene.

[b] Measured in tetrachloroethane and phenol (1:1, wt%) with a concentration of 5 mg/mL at 30 °C.

[c] Determined by ^1H NMR in TFA.

Table S2. Composition of PBST copolyesters.

Sample	Component mol%			Average Sequence length		Degree of randomness
	N_{TBT}	N_{TBS}	N_{SBS}	L_{TBT}	L_{SBS}	R
PBT	100	0.0	0.0	-	-	-
PBST10	68.4	28.4	3.2	5.81	1.21	1.00
PBST20	46.1	43.7	10.2	3.12	1.47	1.00
PBST30	31.8	47.6	20.6	2.33	1.87	0.96
PBST40	20.2	47.7	32.1	1.84	2.34	0.97
PBST50	11.6	48.6	39.8	1.48	2.64	1.05

Table S3. The thermal stability of PBST copolyesters.

Samples	N_2				Air				T_g (℃)
	$T_{d,5\%}$ (℃)	$T_{d,\,max}$ (℃)	$T_{d,1/2}$ (℃)	R_{600} (wt.%)	$T_{d,5\%}$ (℃)	$T_{d,\,max}$ (℃)	$T_{d,1/2}$ (℃)	R_{600} (wt.%)	
PBT	380	411	412	8.5	377	408	405	0	44.1
PBST10	366	412	409	7.7	359	408	404	0	21.3
PBST20	355	412	408	3.9	345	410	403	0	4.4
PBST30	348	412	404	4.1	342	412	401	0	-3.7
PBST40	344	414	401	3.7	341	411	397	0	-10.1
PBST50	340	413	398	3.5	340	406	392	0	-16.3

Table S4 Mechanical Properties of PBST copolyesters.

Sample	E (MPa)	σ_t (MPa)	ε_b (%)	σ_y (MPa)	ε_y (%)
PBT	1550±29	45.2±1.0	405±39	44.8±0.6	4.7±0.2
PBST10	985±21	41.2±1.2	546±30	41.2±0.8	15.7±0.4
PBST20	343±15	20.6±0.8	506±45	19.8±0.5	19.1±0.3
PBST30	138±12	16.8±0.9	770±32	10.5±0.5	23.8±0.5
PBST40	48±2	12.5±0.7	1210±30	5.7±0.2	47.2±0.3
PBST50	5 ± 1	-	702 ± 41	-	-

Table S5. Elastic recovery of PBST copolyesters under 100% strain during cyclic tensile testing.

Sample	R_r (1) (%)	R_r (2) (%)	R_r (3) (%)	R_r (4) (%)	R_r (5) (%)
PBT	7.3 ± 1.2	91.1 ± 0.9	92.9 ± 0.7	94.2 ± 0.3	96.5 ± 0.1
PBST10	17.2 ± 1.1	91.7 ± 1.1	93.6 ± 0.8	94.8 ± 0.7	96.4 ± 0.4
PBST20	24.2 ± 0.9	92.1 ± 0.8	94.1 ± 0.7	95.9 ± 0.3	97.1 ± 0.2
PBST30	43.2 ± 1.0	92.9 ± 0.6	94.9 ± 0.4	96.5 ± 0.2	97.7 ± 0.1
PBST40	60.0 ± 0.8	94.6 ± 0.4	95.8 ± 0.7	97.1 ± 0.2	98.5 ± 0.2
PBST50	81.1 ± 0.8	95.2 ± 0.5	97.3 ± 0.6	98.6 ± 0.3	99.1 ± 0.1

Table S6. Elastic recovery of PBST copolyesters under 200% strain during cyclic tensile testing.

Sample	R_r (1) (%)	R_r (2) (%)	R_r (3) (%)	R_r (4) (%)	R_r (5) (%)
PBT	6.5 ± 1.3	92.3 ± 0.9	94.1 ± 0.7	96.0 ± 0.3	97.0 ± 0.1
PBST10	12.4 ± 1.4	92.9 ± 1.1	94.2 ± 0.9	96.1 ± 0.7	97.0 ± 0.4
PBST20	17.5 ± 0.9	93.4 ± 0.7	95.1 ± 0.6	96.3 ± 0.3	97.1 ± 0.2
PBST30	28.2 ± 1.1	93.8 ± 0.7	95.2 ± 0.3	96.8 ± 0.4	97.4 ± 0.1
PBST40	60.1 ± 0.7	94.9 ± 0.6	96.2 ± 0.5	97.1 ± 0.3	98.1 ± 0.2
PBST50	72.5 ± 0.9	95.2 ± 0.5	96.8 ± 0.4	97.9 ± 0.3	98.4 ± 0.1

Table S7. Comparison of Fe^{3+} chemosensors and their detection limits.

Fluorescent materials	LOD (μM)	Ref.
Porous organic polymer	31.00	1
Organic molecule	6.95	2
NTU-9-NS	0.45	3
UiO-66 rhodamine B	4.16	4
Covalent organic framework	0.17	5
Covalent organic polymer	0.43	6
UiO-66 + coumarin	4.87	7
C-g-PLLA/MCD	3.74	8
C-g-PLLA/DNS-Cl	14.00	9
PBST40	0.71	this work

Table S8. M_n and $Đ$ at different time points during enzymatic degradation of PBST copolyesters.

Degradation Time (Week)	0		2		4	
	M_n (g/mol)	$Đ$	M_n (g/mol)	$Đ$	M_n (g/mol)	$Đ$
PBT	40,000	1.47	40,500	1.47	40,000	1.47
PBST10	49,000	1.75	48,500	1.75	48,500	1.75
PBST20	50,000	1.77	50,000	1.77	49,500	1.77
PBST30	52,000	1.85	52,000	1.85	51,500	1.84
PBST40	51,000	1.81	49,000	1.80	36,000	1.94
PBST50	54,000	1.76	32,000	1.97	9,000	2.14

References

1. L. Guo, X. Zeng, J. Lan, J. Yun and D. Cao, ChemistrySelect, 2017, 2, 1041–1047.
2. X. Gong, H. Zhang, N. Jiang, L. Wang and G. Wang, Micro chem. J., 2019, 145, 435–443.
3. H. Xu, J. Gao, X. Qian, J. Wang, H. He, Y. Cui, Y. Yang, Z. Wang and G. Qian, J. Mater. Chem. A, 2016, 4, 10900–10905.
4. B. Ruan, J. Yang, Y. J. Zhang, N. Ma, D. Shi, T. Jiang and F. C. Tsai, Talanta, 2020, 218, 121207.
5. G. Chen, H. H. Lan, S. L. Cai, B. Sun, X. L. Li, Z. H. He, S. R. Zheng, J. Fan, Y. Liu and W. G. Zhang, ACS Appl. Mater. Interfaces, 2019, 11, 12830–12837.
6. M. Wang, L. Guo and D. Cao, Sci. China: Chem., 2017, 60, 1090–1097.
7. D. Feng, T. Zhang, T. Zhong, C. Zhang, Y. Tian and G. Wang, J. Mater. Chem. C, 2021, 9, 16978–16984.
8. X. B. Yu, Y. T. Xu, F. Liu, W. Zhang, Y. Sun, Y. J. Fang, L. Y. Fang, X. F. He, H. N. Na and J. Zhu, J. Mater. Chem. A, 2023, 11, 23511–23522.
9. X. T. Zhao, Y. Y. Zheng, M. L. Chen, X. Q. Jiang, W. H. Miao, Y. D. Zhao, J. Zhu and F. Liu, Int. J. Biol. Macromol, 2026, 351, 151100.